INTERNATIONAL JOURNAL FOR NUMERICAL METHODS IN FLUIDS, VOL. 22, 515–548 (1996)

A SEGREGATED SOLUTION ALGORITHM FOR INCOMPRESSIBLE FLOWS IN GENERAL CO-ORDINATES

TONY W. H. SHEU AND SHI-MIN LEE*

Institute of Naval Architecture and Ocean Engineering, National Taiwan University, Taipei, Taiwan

SUMMARY

To analyse an incompressible Navier–Stokes flow problem in a boundary-fitted curvilinear co-ordinate system is definitely not a trivial task. In the primitive variable formulation, choices between working variables and their storage points have to be made judiciously. The present work engages contravariant velocity components and scalar pressure which stagger each other in the mesh to prevent even–odd pressure oscillations from emerging. Now that smoothness of the pressure field is attainable, the remaining task is to ensure a discrete divergence-free velocity field for an incompressible flow simulation. Aside from the flux discretizations, the indispensable metric tensors, Jacobian and Christoffel symbols in the transformed equations should be approximated with care. The guiding idea is to get the property of geometric identity pertaining to these grid-sensitive discretizations. In addition, how to maintain the revertible one-to-one equivalence at the discrete level between primitive and contravariant velocities is another theme in the present staggered formulation. A semi-implicit segregated solution algorithm felicitous for a large-scale flow simulation was utilized to solve the entire set of basic equations iteratively. Also of note is that the present segregated solution algorithm has the virtue of requiring no user-specified relaxation parameters for speeding up the satisfaction of incompressibility in an optimal sense. Three benchmark problems, including an analytic problem, were investigated to justify the capability of the present formulation in handling problems with complex geometry. The test cases considered and the results obtained herein make a useful contribution in solving problems subsuming cells with arbitrary shapes in a boundary-fitted grid system.

KEY WORDS: incompressible; Navier–Stokes; contravariant velocities

1. INTRODUCTION

In fluid engineering, numerous problems of practical relevance are centred around the incompressible Navier–Stokes equations. To develop a computer program capable of simulating this class of fluid flows in an arbitrary domain is definitely beneficial to many industrial societies. A multitude of efforts have been made by researchers in the community of computational fluid dynamics. With the advent of modern computers, this technique is slowly emerging as a substitute for much more expensive experimental calibration.

Simulation quality for an incompressible fluid flow can be evaluated from several viewpoints such as solution accuracy and stability. Aside from the prediction error arising from the flux discretization, an

* Present address: Institute of Aeronautical Engineering, Tamkang University, Tamsui, Taipei, Taiwan.

CCC 0271–2091/96/060515-34

Received 24 February 1994
Revised 5 May 1995

inevitable evaluation of metric tensors is another major source of errors when a boundary-fitted, non-orthogonal co-ordinate transformation is conducted in the finite difference setting. Unless one uses a non-co-ordinate-invariant approach,[1] an attempt to model these geometric quantities turns out to be indispensable in the hope of retaining good solution accuracy in a non-uniform mesh with substantial grid skewness. Discretization errors originating from these curvature terms can be largely reduced to the satisfaction of physical reality if rules can be followed. How to manipulate these geometric quantities appearing in the transformed equations will be considered in this paper. We are also aiming at enhancing the scheme stability, together with high-order solution accuracy, so that the developed computer programme can be used over and over in predicting industrial flows.

To conduct a large-scale flow simulation, direct approaches[2] are not advantageous in the sense of both execution time and memory storage as compared with segregated approaches.[3] This has led many authors to analyse the entire differential system iteratively in an *ad hoc* manner. Inspired by the pioneering works of Harlow and Welch[4] and Chorin,[5] which can be interpreted as operator-splitting or fractional step methods, many decoupled methods for the solution of incompressible flow equations were developed later. In this class of methods the guiding idea is to employ a two-step time discretization for the conservation equations so that the primitive pressure variable can be decoupled from the momentum equations.[6] The intermediate velocity can be projected onto a subspace of divergence-free vectors. This projection theory works effectively only for the time-dependent incompressible Navier–Stokes flow analysis. If one is only concerned with the steady state solution, the segregated approach of Patankar[7] will be more attractive. The pressure gradients still serve as the source terms in the momentum calculations.

2. THEORETICAL FORMULATION

In the open literature the primitive variable (velocity–pressure),[8] streamfunction–vorticity[9] and velocity–vorticity[10] formulations are three major settings of dependent variables that have been commonly used in incompressible viscous flow simulations. Each formulation has certain advantages. In every aspect an overwhelming superiority of one method over the other two has not been clearly demonstrated. The present analysis is based on the velocity–pressure formulation, so that the physics of the fluid flow taking place in a Cartesian system can be analysed by solving the following tensor form of the conservation equations:

$$\frac{\partial}{\partial t}(\rho) + \frac{\partial}{\partial x_j}(\rho u_j) = 0, \tag{1a}$$

$$\frac{\partial}{\partial t}(\rho u_i) + \frac{\partial}{\partial x_j}(\rho u_j u_i) = -\frac{\partial P}{\partial x_i} + \frac{\partial}{\partial x_j}\left(\mu \frac{\partial u_i}{\partial x_j}\right) + \frac{\partial}{\partial x_j}\left(\mu \frac{\partial u_j}{\partial x_j}\right), \tag{1b}$$

where u_i are the Cartesian velocity components. In dimensional form P is the pressure, ρ the density and μ the dynamic viscosity.

With the aid of a boundary-fitted co-ordinate (BFC) transformation[11] it was possible to simulate a realistic flow problem by using a finite difference or finite volume method. This technique is the subject of intensive numerical research and has been applied to a wide variety of flow problems. The reason for this increased activity of making use of non-orthogonal co-ordinates rather than the classical orthogonal co-ordinates is grounded in its flexibility of representing a complex geometry. The governing equations (1a, b) are first transformed to those in a curvilinear co-ordinate system and then discretized in a rectangular grid system. After conducting a series of chain rule manipulations, the governing equations (1a, b) can be represented in a general non-orthogonal curvilinear co-ordinate

system as

$$\frac{\partial}{\partial t}(\rho) + (\rho u^j)_{,j} = 0, \tag{2a}$$

$$\frac{\partial}{\partial t}(\rho u^i) + (\rho u^k u^i)_{,k} = -g^{ik}\frac{\partial P}{\partial \xi^k} + g^{kr}(\mu u^i)_{,kr}. \tag{2b}$$

To date, a large variety of numerical models have been proposed, analysed, discretized and evaluated for incompressible viscous flows. The velocity–pressure formulation has gained wide acceptance, presumably because it involves the variables of most interest in industrial flows. In this context, Cartesian,[12] contravariant,[13,14] covariant[15] velocity components and physical contravariant velocities[16] could be chosen as the dependent variables for the transformed basic equations. Besides these, a mathematical model using the contravariant velocity along the flow direction and the other two primitive velocities in the transverse co-ordinate plane was also proposed.[17] While the use of primitive velocities could render simpler conservation equations, it is subject to erroneous prediction, since the flow is not aligned well with the grid lines in a curved grid. As for the covariant velocities, they tend to couple with the pressure but at the expense of yielding a more complex discrete flux expression. For the contravariant velocity and its physical components the difficulties are reversed. Physical components of the contravariant vector are particularly attractive when the analysis is carried out on a non-uniform grid, since the derivative of a contravariant component becomes non-zero even if the flow velocity is uniform. Contravariant velocity components have been applied by one of the present authors to analyse both parabolized Navier–Stokes equations[18] and Navier–Stokes equations.[19] The present work is a continuation of this previous work. We prefer to use contravariant rather than covariant components, mainly because the transformed convective and diffusive fluxes in a curvilinear system bear a resemblance to those formulated in a Cartesian co-ordinate system. Many effective solution algorithms that are available in the Cartesian context can consequently be employed safely. The inferiority of the underlined contravariant velocity to the physical contravariant components will be circumvented in the present study.

The basic equations represented in a strong conservation law form are obtained by firstly multiplying equations (1a, b) by the transformation Jacobian determinant (J) and then using the metric identity $(\partial/\partial\xi_m)(J\partial\xi_m/\partial x_j) = 0$ to bring the product $J\partial\xi_m/\partial x_j$ inside the partial differentiations of every convective and diffusive term in the equation set.[20] This manipulation results in the following transformed equations, where U and V serve as the dependent variables for the ξ- and η-momentum equations respectively:

$$\frac{\partial}{\partial t}(\rho J\phi) + \frac{\partial}{\partial \xi}(\rho JU\phi) + \frac{\partial}{\partial \eta}(\rho JV\phi) = -P^\phi + \frac{\partial}{\partial \xi}\left(\Gamma^\phi Jg^{11}\frac{\partial \phi}{\partial \xi}\right) + \frac{\partial}{\partial \eta}\left(\Gamma^\phi Jg^{22}\frac{\partial \phi}{\partial \eta}\right) + S_2^\phi + S_3^\phi, \tag{3}$$

where

	ϕ	Γ^ϕ	P^ϕ	S_2^ϕ	S_3^ϕ
continuity	1	0	0	0	0
ξ-momentum	U	μ	$J(P_\xi g^{11} + P_\eta g^{12})$	$\frac{\partial}{\partial \xi}\left(\mu Jg^{12}\frac{\partial U}{\partial \eta}\right) + \frac{\partial}{\partial \eta}\left(\mu Jg^{21}\frac{\partial U}{\partial \xi}\right)$	$S_{31}^U - S_{32}^U - S_{33}^U$
η-momentum	V	μ	$J(P_\xi g^{12} + P_\eta g^{22})$	$\frac{\partial}{\partial \xi}\left(\mu Jg^{12}\frac{\partial V}{\partial \eta}\right) + \frac{\partial}{\partial \eta}\left(\mu Jg^{21}\frac{\partial V}{\partial \xi}\right)$	$S_{31}^V - S_{32}^V - S_{33}^V$

and

$$S_{31}^{U_k} = (\rho JUu)(\varepsilon_x^k)_\xi + (\rho JUv)(\varepsilon_y^k)_\xi + (\rho JUu)(\varepsilon_x^k)_\eta + (\rho JUv)(\varepsilon_x^k)_\eta, \tag{4a}$$

$$S_{32}^{U_k} = \left[\mu J\left(g^{11}\frac{\partial u}{\partial \xi} + g^{12}\frac{\partial u}{\partial \eta}\right)\right](\varepsilon_x^k)_\xi + \left[\mu J\left(g^{11}\frac{\partial v}{\partial \xi} + g^{12}\frac{\partial v}{\partial \eta}\right)\right](\varepsilon_y^k)_\xi + \left[\mu J\left(g^{21}\frac{\partial u}{\partial \xi} + g^{22}\frac{\partial u}{\partial \eta}\right)\right](\varepsilon_x^k)_\eta + \left[\mu J\left(g^{21}\frac{\partial v}{\partial \xi} + g^{22}\frac{\partial v}{\partial \eta}\right)\right](\varepsilon_y^k)_\eta, \tag{4b}$$

$$S_{33}^{U_k} = \frac{\partial}{\partial \xi}[\{\mu Ju[g^{11}(\varepsilon_x^k)_\xi + g^{12}(\varepsilon_x^k)_\eta]\} + \{\mu Jv[g^{11}(\varepsilon_y^k)_\xi + g^{12}(\varepsilon_y^k)_\eta]\}] + \frac{\partial}{\partial \eta}[\{\mu Ju[g^{21}(\varepsilon_x^k)_\xi + g^{22}(\varepsilon_x^k)_\eta]\} + \{\mu Jv[\{g^{21}(\varepsilon_y^k)_\xi + g^{22}(\varepsilon_y^k)_\eta]\}]], \tag{4c}$$

$$g^{11} = \frac{\alpha}{J^2}, \qquad g^{12} = g^{21} = -\frac{\beta}{J^2}, \qquad g^{22} = \frac{\gamma}{J^2},$$

$$\alpha = x_\eta^2 + y_\eta^2, \qquad \beta = x_\xi x_\eta + y_\xi y_\eta, \qquad \gamma = x_\xi^2 + y_\xi^2,$$

$$J = x_\xi y_\eta - x_\eta y_\xi, \qquad \varepsilon^1 = \xi, \qquad \varepsilon^2 = \eta.$$

The velocity components defined in the (x, y) co-ordinate system map to the computational co-ordinate system via the following one-to-one relations:

$$U = \xi_x u + \xi_y v, \qquad V = \eta_x u + \eta_y v. \tag{5}$$

The strong resemblance between equations (2) and (3) enables us to adopt a solution algorithm that has been successfully developed in the Cartesian co-ordinate system and apply it directly to its curvilinear counterpart.

3. DISCRETIZED CONVECTION SCHEME

Typically, the existing multidimensional upwind schemes were developed by modifying an *ad hoc* one-dimensional scheme through the space-operator-splitting procedure.[21] This gives rise to a so-called numerical diffusion error featuring the lowest order of mixed derivative term in the modified equation. Numerical inaccuracy of this type might mask the real physics regardless of the accuracy order of the employed scheme. The deterioration accuracy is especially severe when the flow is not aligned well with the grid lines. To exploit a truly multidimensional advection scheme is consequently essential provided that the solution sought is of high quality.[22] This paper aims at presenting a quadratic upwind two-dimensional advection scheme in an attempt to reduce the computed inaccuracy stemming from the dimensional splitting. The underlying philosophy in designing the present advection scheme is to take the flow direction into consideration.

For the sake of simplicity we consider a pure convection equation in this regard:

$$\frac{\partial \phi}{\partial t} + u\frac{\partial \phi}{\partial x} + v\frac{\partial \phi}{\partial y} = 0. \tag{6}$$

Also, for the sake of ease of analysis, both velocity components are assumed to be positive. Referring to Figure 1, we utilize 10 nodal points to represent the discrete transport of equation (6):

$$\frac{\phi_P^{n+1} - \phi_P^n}{\Delta t}\Delta x \Delta y + (F_r\phi_r - F_l\phi_l + F_t\phi_t - F_b\phi_b)^{n+1} = 0, \tag{7}$$

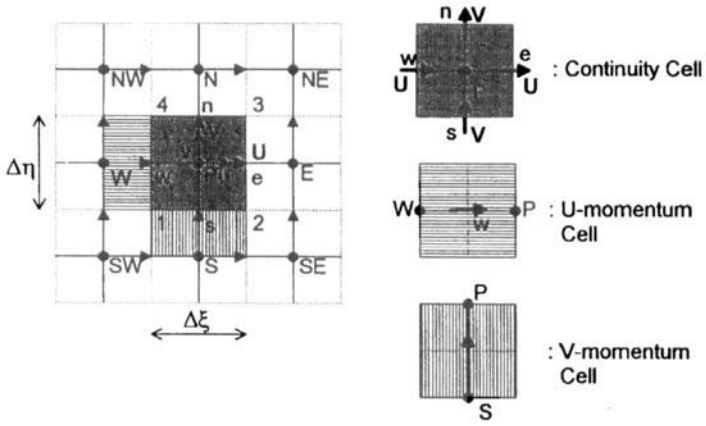

Figure 1. Lay-out of staggered grid system

where

$$F_r = u_E \Delta y, \qquad F_l = u_P \Delta y, \qquad F_t = v_N \Delta x, \qquad F_b = v_p \Delta x,$$

$$\phi_r^{n+1} = \phi_{UD_r}^{n+1} + S_{HD_r}^n, \qquad \phi_{UD_r}^{n+1} = \phi_P, \qquad S_{HD_r}^n = \tfrac{1}{8}(3\phi_E - \phi_W - \phi t_N - \phi_S),$$

$$\phi_l^{n+1} = \phi_{UD_l}^{n+1} + S_{HD_l}^n, \qquad \phi_{UD_l}^{n+1} = \phi_W, \qquad S_{HD_l}^n = \tfrac{1}{8}(3\phi_P - \phi_{WW} - \phi_{NW} - \phi_{SW}),$$

$$\phi_t^{n+1} = \phi_{UD_t}^{n+1} + S_{HD_t}^n, \qquad \phi_{UD_t}^{n+1} = \phi_P, \qquad S_{HD_t}^n = \tfrac{1}{8}(3\phi_N - \phi_S - \phi_E - \phi_W),$$

$$\phi_b^{n+1} = \phi_{UD_b}^{n+1} + S_{HD_b}^n, \qquad \phi_{UD_b}^{n+1} = \phi_S, \qquad S_{HD_b}^n = \tfrac{1}{8}(3\phi_P - \phi_{SS} - \phi_{SE} - \phi_{SW}).$$

This partial implicit discretization formulation falls within the category of interface-based upwind schemes where the invoked stencil points are not necessarily distributed only on the co-ordinate lines passing through the reference point P. Hereinafter we designate the above advection scheme as the 1/8 QUICK scheme. Detailed discussion of it may be found in Reference 23.

4. SOLUTION ALGORITHM

Existing methods which solve the pressure–velocity coupled system (1) encounter two notorious difficulties: (i) the presence of odd–even pressure oscillations and (ii) the enforcement of the discrete continuity equation to machine error. A discretization formulated on staggered grids, such as those implemented in SIMPLE,[7] MAC[4] and ALE,[24] is a remedy for the first difficulty. These unphysical decoupling oscillations can also be suppressed in a non-staggered or collocated grid[25] by imposing a necessary compatibility condition in an integral–differential form. A strong point in favour of the collocation approach is its logical simplicity. It is, however, not a straightforward task from the viewpoints of mathematical derivation and numerical implementation. As a consequence, we adopt a cell centre scheme where unknowns are stored at the centre of each representative control volume to circumvent these checkerboard pressure oscillations. As shown in Figure 1, it involves a group of three control volumes, two for each contravariant velocity and one for the pressure. The mixed formulation is a trivial remedy for the second difficulty. The disk storage required, however, can be considerable and in many cases may be insurmountable based on the state of the art in computer technology. It poses a severe limitation in multidimensional computations. We are therefore led to the segregated approach which will be discussed later in this section.

By integrating the conservation equations over their respective quadrilateral cells, together with use of the divergence theorem, one can convert the partial differential equations to integral form. Each momentum equation in its respective control volume thus can be discretized as follows:

ξ-momentum equation,

$$U_w = U_w^* + \alpha_w^U \left(\frac{C_e U_e + C_{Nw} U_{Ww} + C_{Nw} U_{Nw} + C_{Sw} U_{Sw} + b_w + a_w}{C_w} - U_w^* \right); \tag{8}$$

η-momentum equation,

$$V_s = V_s^* + \alpha_s^V \left(\frac{C_{sE} V_{sE} + C_{sW} V_{sW} + C_n V_n + C_{Ss} V_{Ss} + b_s + a_s}{C_s} - V_s^* \right). \tag{9}$$

Hereinafter we use a superscript asterisk to denote the previous iteration step. While the relaxation factors α^U and α^V are important in effectively reducing the momentum residuals, we assign them to be constant ($\alpha^U = \alpha^V = 0{\cdot}8$). The pursuit of an optimal relaxation procedure is under way.

For solving a large-scale problem with a traditional computer, one has a preference for a projection method[26,27] or the simplified marker- and-cell method[28] which have been developed underlying the concept of Chorin.[5] In these methods one can split the numerical operator and achieve pressure–velocity coupling through solving a Poisson-like elliptic equation for either the pressure[29] or the pressure correction.[3] Since this concept is not applicable to steady state analyses, a segregated approach, with first-order accuracy in time, of the SIMPLE type[3] will be employed herein.

From a guessed pressure field we have no difficulty solving for the contravariant velocities from the momentum equations in succession. These computed velocities violate the divergence-free constraint condition and in turn reflect in the pressure field.[28] The strategy to correct these erroneous pressures consequently must take this constraint condition or continuity equation into account. By bearing this in mind, a Poisson equation is derived as

$$a_P P'_P = a_E P'_E + a_W P'_W + a_N P'_N + a_S P'_S + b, \tag{10}$$

where

$$a_E = (\rho J d)_e \Delta\eta, \qquad a_W = (\rho J d)_w \Delta\eta, \qquad a_N = (\rho J d)_n \Delta\xi, \qquad a_S = (\rho J d)_s \Delta\xi,$$

$$d_e = \frac{J_e (\delta\xi)_e \Delta\eta}{a_e^U - \sum a_{nb}^U}, \qquad d_w = \frac{J_w (\delta\xi)_w \Delta\eta}{a_w^U - \sum a_{nb}^U}, \qquad d_n = \frac{J_n (\delta\eta)_n \Delta\xi}{a_n^V - \sum a_{nb}^V}, \qquad d_s = \frac{J_s (\delta\eta)_s \Delta\xi}{a_s^V - \sum a_{nb}^V},$$

$$b = \frac{[(\rho J)_P^0 - (\rho J)_P]\Delta\xi\Delta\eta}{\Delta t} + [(\rho J U^*)_W - (\rho J U^*)_e]\Delta\eta + [(\rho J V^*)_s - (\rho J V^*)_n]\Delta\xi$$
$$+ a_E g^{12} P'_\eta|_e - a_W g^{12} P'_\eta|_w + a_N g^{21} P'_\xi|_n - a_S g^{21} p'_\xi|_s.$$

The above positive definite matrix equation for the pressure correction can be solved effectively either by the well-known Thomas direct solver or by a variant of conjugate gradient iterative solvers along with a boundary condition $P' = 0$ of the Dirichlet type.

As is common practice, this semi-implicit coupling solution algorithm is also sensitive to the preassigned values of pressure. One thus has to cope with this problem by devising an effective relaxation procedure for velocities. The demand on a relaxation procedure for the pressure is also great and calls for a refined approach.[30] One way to correct the pressure field is to add a fraction α^P of P' to the previously computed pressure field P^*:

$$P = P^* + \alpha^P P'. \tag{11}$$

Since α^P determines the rate of discrete divergence towards machine zero, it is not encouraged by assigning the value of α^P by experience. In the present study we are to reduce the global residual

$$G^2 = \sum_{\text{all nodes}} (R_u^2 + R_v^2) \tag{12}$$

in the course of segregated processes. The ingredients chosen in the above momentum reductions take the forms

$$R_u = c_e U_e - \sum c_{nb} U_{nb} - S_u - A_e^1(P_P^* - P_E^*) - A_e^2(P_{Se}^* - P_{Ne}^*), \tag{13}$$

$$R_v = c_n V_n - \sum c_{nb} V_{nb} - S_v - A_n^1(P_P^* - P_N^*) - A_n^2(P_{Nw}^* - P_{Ne}^*). \tag{14}$$

The relaxation factor α^P is obtained by setting $\partial G^2/\partial \alpha^P = 0$ to minimize the error.[31] It leads to the following spatially independent expression for α^P:

$$\alpha^P = \frac{\sum\{R_u[A_e^1(P'_p - P'_E) + A_e^2(P'_{Se} - P'_{Ne})] + R_v[A_n^1(P'_P - P'_N) + A_n^2(P'_{Nw} - P'_{Ne})]\}}{\sum\{[A_e^1(P'_P - P'_E)]^2 + [A_e^2(P'_{Se} - P'_{Ne})]^2 + [A_n^1(P'_P - P'_N)]^2 + [A_n^2(P'_{Nw} - P'_{Ne})]^2\}}. \tag{15}$$

In response to the above-mentioned pressure change, the velocities are then corrected accordingly:

$$U_e = U_e^* - d_e(g^{11}P'_\xi + g^{12}P'_\eta)_e, \qquad V_n = V_n^* - d_n(g^{21}P'_\xi + g^{22}P'_\eta)_n. \tag{16}$$

One can repeat the above computational procedures using the updated pressure to solve for the contravariant velocities, until each momentum residual reaches the user-specified convergence tolerance.

5. CALCULATION OF GEOMETRIC COEFFICIENT TERMS

Comparing the Navier–Stokes equations formulated in two different co-ordinate systems, they are virtually invariant after the curvilinear co-ordinate transformation has been made. In the transformed equations (2) the transformation production terms featuring the mesh distortion, however, are rather memory-intensive and cumbersome to compute. These geometric quantities require differentiation of mapping once or twice. Owing to the necessity of computing Christoffel symbols, contravariant metric tensors and base vectors, the solution accuracy depends largely on the discretization schemes for these geometric quantities. As a consequence, any flow simulation involving contravariant velocity components is under the influence of grid uniformity and skewness. We have felt the need for a treatise that these two issues must be well taken care of when using the present contravariant velocity formulation.

On non-orthogonal grids, two basic guidelines leading to physically plausible meanings have been proposed.[32] The first requirement deals with the discrete level of the geometric identity. To achieve this goal, we integrate the transformed continuity equation over a continuity cell:

$$\int\int\left(\frac{\partial}{\partial\xi}(JU) + \frac{\partial}{\partial\eta}(JV)\right)\mathrm{d}\xi\,\mathrm{d}\eta = 0. \tag{17}$$

With the help of the divergence theorem this surface integral can be analytically converted to the line integral

$$\oint (JU\,\mathrm{d}\eta + JV\,\mathrm{d}\xi) = 0 \tag{18}$$

or

$$\oint u(y_\eta\,\mathrm{d}\eta - y_\xi\,\mathrm{d}\xi) + v(x_\xi\,\mathrm{d}\xi - x_\eta\,\mathrm{d}\eta) - 0. \tag{19}$$

In cells of arbitrary shape the above expression can be furthermore approximated as follows, assuming the case considered involves a constant velocity vector (u, v):

$$\oint y_\eta \, d\eta - y_\xi \, d\xi = 0 \tag{20}$$

or

$$\oint x_\xi \, d\xi - x_\eta \, d\eta = 0. \tag{21}$$

These equations provide us with good knowledge of handling grid-sensitive terms such as x_ξ, x_η, y_η and y_ξ. It is important to note that equations (20 and 21) deal only with the differentiation of mapping a cell, shown in Figure 2. Co-ordinate values other than those in the investigated cell have nothing to do with the evaluations of these geometric quantities. As an example of this observation we can compute x_ξ, x_η, y_η and y_ξ from the underlying interpolation theory:

$$x = \sum_{i=1}^{9} N_i x_i, \qquad y = \sum_{j=1}^{9} N_i y_i, \tag{22}$$

where $N_i(m, n)$ are known as biquadratic shape functions.[33] Use of the above mapping yields

$$\begin{bmatrix} \dfrac{\partial x}{\partial \xi} & \dfrac{\partial x}{\partial \eta} \\ \dfrac{\partial y}{\partial \xi} & \dfrac{\partial y}{\partial \eta} \end{bmatrix} = \begin{bmatrix} \displaystyle\sum_{i=1}^{9} \frac{\partial N_i}{\partial \xi} x_i & \displaystyle\sum_{j=1}^{9} \frac{\partial N_i}{\partial \eta} x_i \\ \displaystyle\sum_{j=1}^{9} \frac{\partial N_i}{\partial \xi} y_i & \displaystyle\sum_{j=1}^{9} \frac{\partial N_i}{\partial \eta} y_i \end{bmatrix}. \tag{23}$$

By substituting these biquadratic shape functions $N_i(m, n)$ into equations (23), the discrete levels of (20) and (21) are reached.

Another crucial issue, which might even cause substantial errors in a uniform velocity field, has been reported in a grid system where an abrupt change in mesh density exists.[34] Under this simple flow condition the discrete equation can be exactly satisfied by using the physical contravariant velocity components.[35] This highlights the importance of evaluating the Cartesian velocity components from their corresponding working variables (contravariant velocity components). It necessitates the development of an interpolation method for surmounting numerical difficulties in regions with an abrupt change in mesh size.

By definition, U and V are given by equation (5). Analytically, these relations amount to

$$u = J(\eta_x U - \xi_y V), \qquad v = J(-\eta_x U + \zeta_x V). \tag{24}$$

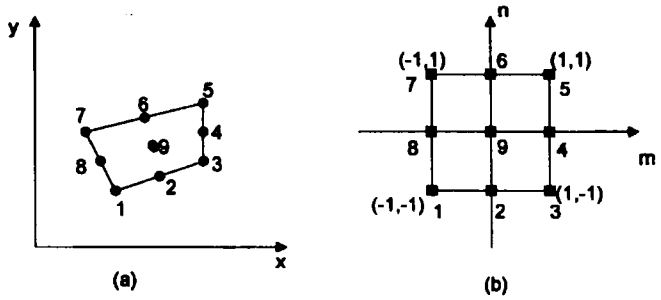

Figure 2. Transformation from a physical cell in (a) to a rectangular computational cell in (b)

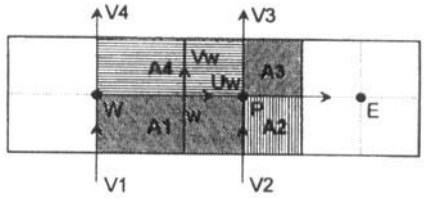

Figure 3. Location of velocity nodes

Because of the staggered nature, we have to interpolate the value of V when calculating u and likewise to interpolate the value of U when calculating v. Referring to Figure 3, the area-weighted interpolation scheme is used to compute the contravariant velocity component, for example, on the west side of the control surface:

$$V_w = \frac{V_1A_1 + V_2A_2 + V_3A_3 + V_4A_4}{A_1 + A_2 + A_3 + A_4}. \tag{25}$$

Once the contravariant velocity component U_w becomes available, one can compute the Cartesian velocity (u, v) at the grid point 'w' from

$$u_w = J_w(\eta_x|_w U_w - \xi_y|_w V_w), \qquad v_w = J_w(-\eta_x|_w U_w + \xi_x|_w V_w). \tag{26}$$

For the sake of a clear illustration of the underlying concept, we briefly summarize the procedures that yield the values of (u, v) from the available setting (U, V).

(i) Given an analytic Cartesian velocity field (u, v).
(ii) Set up an analytic grid distribution so that the geometry coefficients can be exactly computed.
(iii) Calculate the contravariant velocity field (U, V) from the transformation relations shown in equation (5).
(iv) Interpolate the value of V when calculating u and the value of U when calculating v from equation (24) by the present algorithm.
(v) Compare the solutions from step (iv) with the exact solutions given in (i).

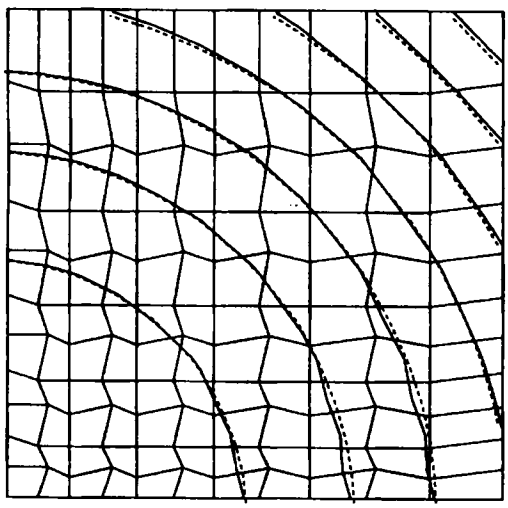

Figure 4. Comparison of contour plots of U-velocity between computed (———) and analytic (— — —) results

To facilitate the assessment of the proposed area-weighted interpolation, we have worked on the velocity field

$$u = v = x^2 + y^2 \tag{27}$$

and the analytic mapping $(x, y) \rightarrow (\xi, \eta)$,

$$x(\xi) = \frac{\sinh(a\xi)}{\sinh(a)}, \qquad y(\eta) = \frac{\sinh(a\eta)}{\sinh(a)}. \tag{28}$$

The test case considered and the results shown in Figure 4 validate the effectiveness of the present procedures in dealing with the velocity transformation in a skewed grid system.

6. COMPUTED RESULTS

For the flux terms and metric tensors, several examples are given below showing the utility of the proposed method in handling problems with arbitrarily discretized cells. In these calculations the effects of the Reynolds number, grid concentration and relaxation factor on the simulation quality were taken into account.

6.1. Navier–Stokes equations with analytic solutions

The first case is that of an analytic problem defined in a rectangular domain $0 \leqslant x, y \leqslant 1$. The incompressible Navier–Stokes equations are solved on several continuously refined grids. At the boundary points the velocities are specified according to the analytic expressions

$$u = -y, \tag{29}$$

$$v = x. \tag{30}$$

With these the analytic pressure distribution in the physical domain is given by

$$p = \tfrac{1}{2}(x^2 + y^2). \tag{31}$$

In this problem, attention was directed to confirming whether the proposed schemes work in approximating non-linear advective fluxes and metric tensors. Figure 5 plots the contours of pressure error obtained on a mesh containing 80×80 nodal points. The good agreement between the analytic and numerical results indicates the reliability of the numerical analysis.

On the basis of computed solutions at nodal points starting from 20×20 to 80×80, a mesh sensitivity analysis was also conducted for $Re = 1000$. Figure 6 shows the residual reduction against the continuously refined grid size, from which the rates of convergence are 1·956 and 1·997 for the velocity and pressure respectively. In the present calculation the convergence criterion consisted of ensuring that the largest normalized residuals for the three conservation equations were less than 10^{-6}. By invoking the Lax equivalent theorem, the numerical stability is ensured, as the scheme presented meets the conditions of convergence and consistency.

The next two cases involve problems of internal and inflow–outflow types. Although their analytic solutions are not available, these problems are presented to confirm the capability of the finite volume code in handling problems with arbitrarily discretized cells.

6.2. Laminar flow in a skew-driven cavity

First we considered an incompressible fluid flow in a tilted cavity as shown in Figure 7, which is depicted by a parallelogram of length $L = 1$. This problem has received wide attention because the domain discretization is easily implemented.

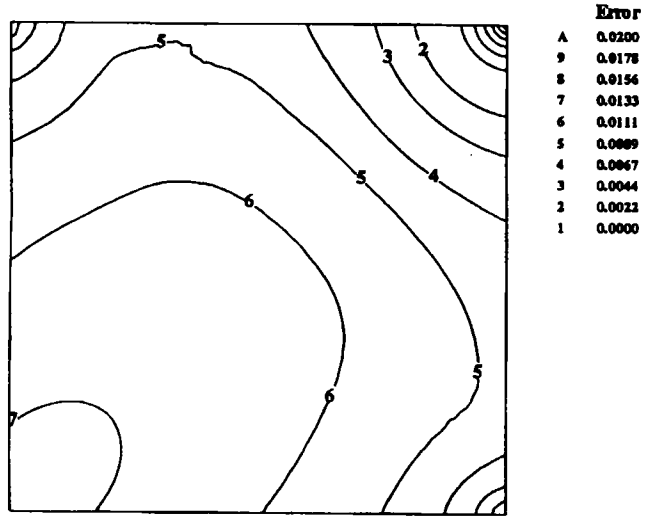

Figure 5. Error contours for pressure

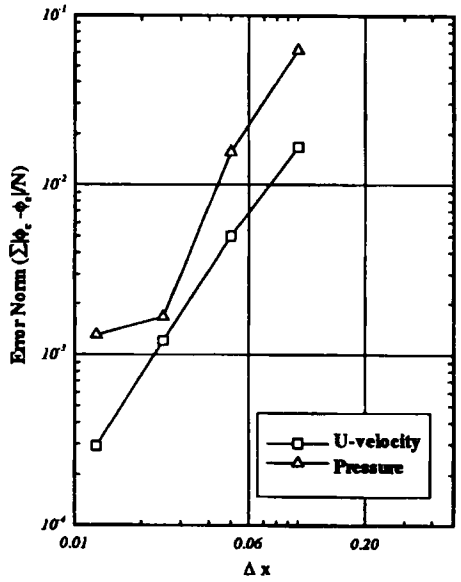

Figure 6. Error reductions for velocity and pressure at different grid sizes

We divided the physical domain into two families of mesh lines parallel to one of the disconnected boundaries. Two tilt angles, $\theta = \pi/4$ and $\pi/6$, were investigated. This leads to a uniform but non-orthogonal grid system. Boundary conditions of the Dirichlet type are imposed at the cavity wall. We specified $u = v = 0$ everywhere except at the upper boundary, where $u = 1$, $v = 0$. Solutions were sought at Reynolds numbers of 100 and 1000. In order to ensure that grid-independent results are attained, a continuous refinement consisting of 21 × 21, 41 × 41 and 81 × 81 cells is necessary.

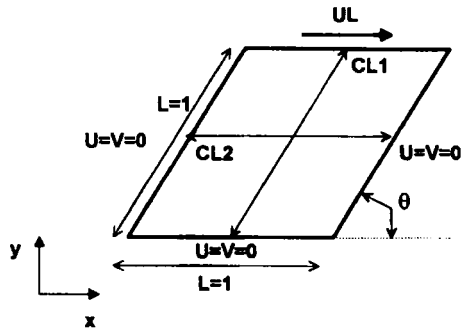

Figure 7. Schematic diagram of a tilt cavity

Figure 8 shows the Cartesian velocity distributions along the centreline CL1 for u and the centreline CL2 for v, together with comparison results given by Demirdzic *et al.* for $Re = 100$.[36] As seen From Figure 8, the predicted u in a cavity of tilt angle $\theta = 30°$ approaches that of Demirdzic *et al.*[36] for a 320 × 320 grid system. We also plotted the computed velocities along the centrelines CL1 and CL2 in Figure 9 to study the influence of the Reynolds number on the grid dependence. Both tilt angles have been investigated. By comparing the computed data in Figures 8 and 9 for different angles $\theta = 30°$ and 45°, we found that the grid dependence seems to exhibit an asymptotic behaviour for the lower Reynolds number. Figure 10 depicts two types of convergence histories against the iteration number. Noticeable is the wavy route of the error reduction for the maximum mass residuals. Such a convergence history is believed to be associated with the eigensystem of the coefficient matrix. The effects of the grid density, grid skewness and Reynolds number on the solution stability are summarized as follows based on the plots shown in Figure 10: with increasing grid numbers, Reynolds number and grid skewness the rate of convergence tends to decrease. We also plotted the kinematic energy inside the cavity against the iteration number at different grid densities in Figure 11 to demonstrate the attainable convergent solution (or steady state).

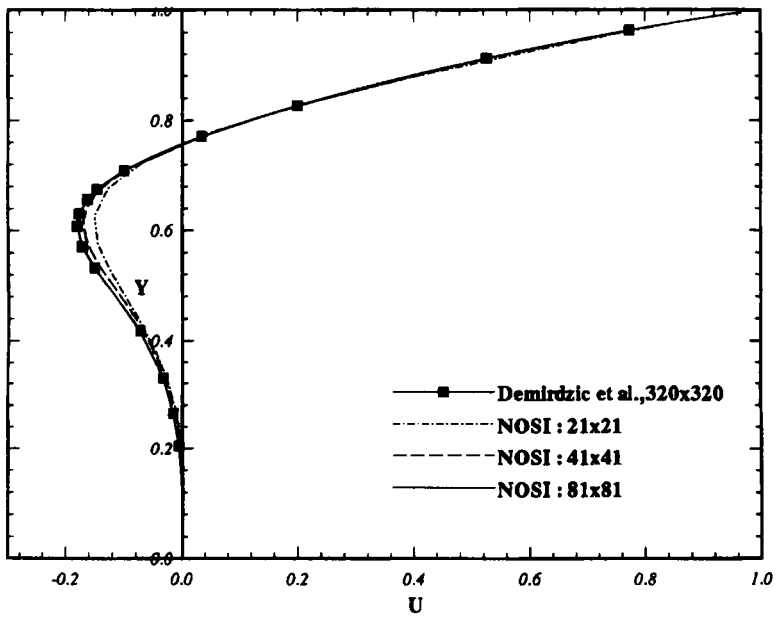

Figure 8(a). Velocity profiles of u along CL1 against grid density for $\theta = 30°$ and $Re = 100$

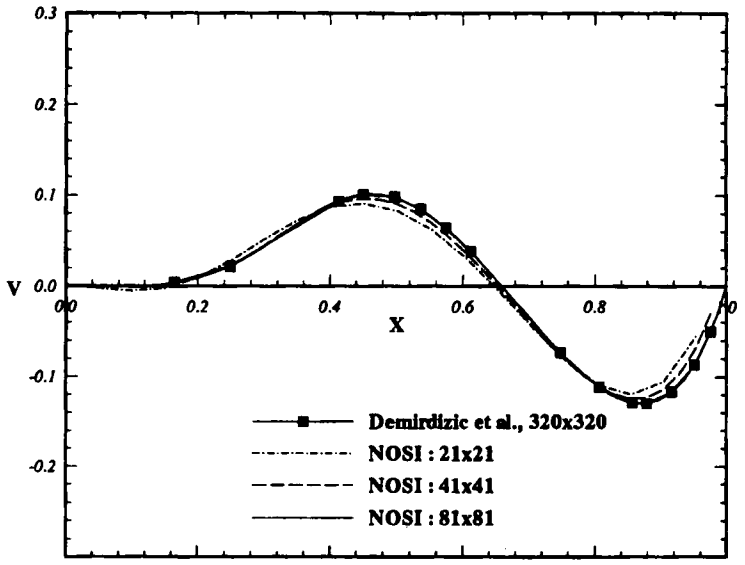

Figure 8(b). Velocity profiles of v along CL2 against grid density for $\theta = 30°$ and $Re = 100$

In a fixed domain the physical complexity has a close relation with the high Reynolds number. A test problem of higher Reynolds number should therefore be analysed to ensure that the numerical solution converges correctly. With this reasoning a flow condition of $Re = 3200$ was considered in a square cavity instead of the skew cavity owing to the lack of comparison data. The error reduction, illustrated in Figure 12, still proceeds quite well. For the sake of comparison in accuracy we also plotted the converged solutions in Figure 13, which agree well with those of Ghia *et al.*[37]

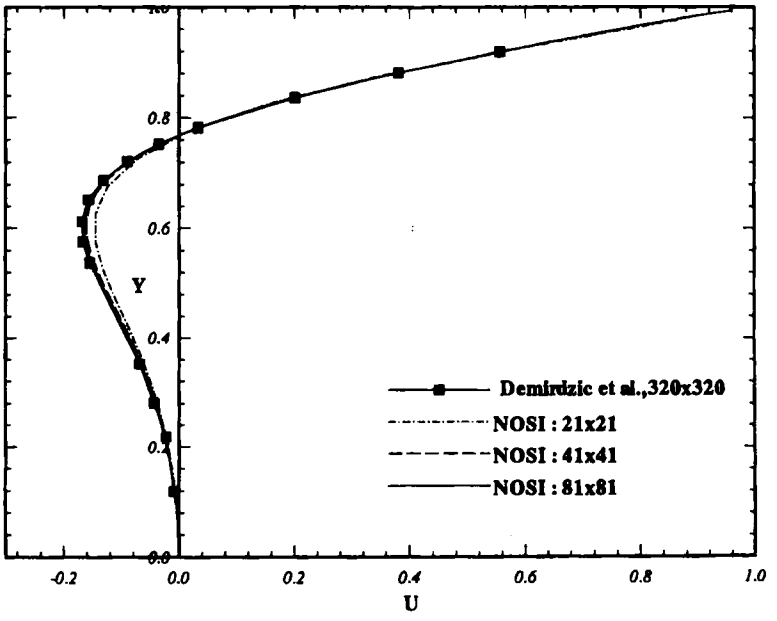

Figure 8(c). Velocity profiles of u along CL1 against grid density for $\theta = 45°$ and $Re = 100$

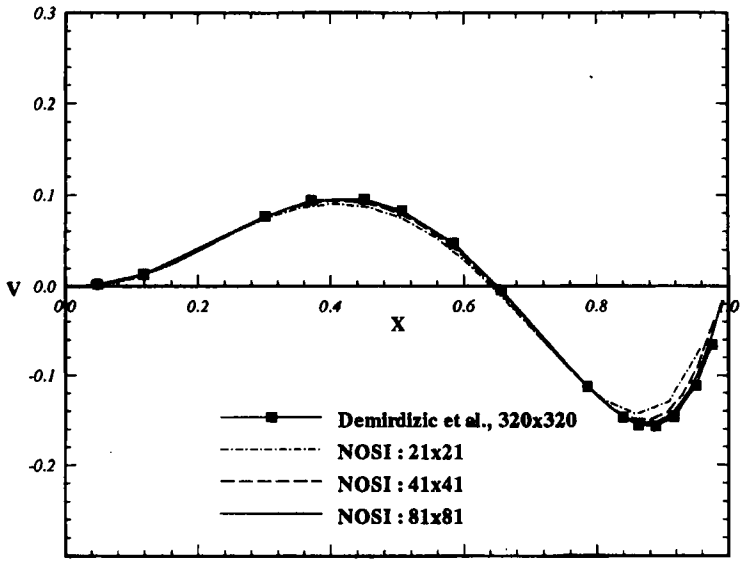

Figure 8(d). Velocity profiles of v along CL2 against grid density for $\theta = 45°$ and $Re = 100$

The importance of relaxing the investigated elliptic system is best illustrated by plotting the relaxation factor for the pressure, on the basis of the rationale given in equation (15), against the iteration number as in Figure 14. From the computed relaxation factors we can conclude that the values of the relaxation factor change more rapidly with increasing Reynolds number and tilt angle. On the contrary, as the grid number increases, the relaxation parameters seem to vary in a mild manner provided that the grid skewness and Reynolds number are kept unchanged.

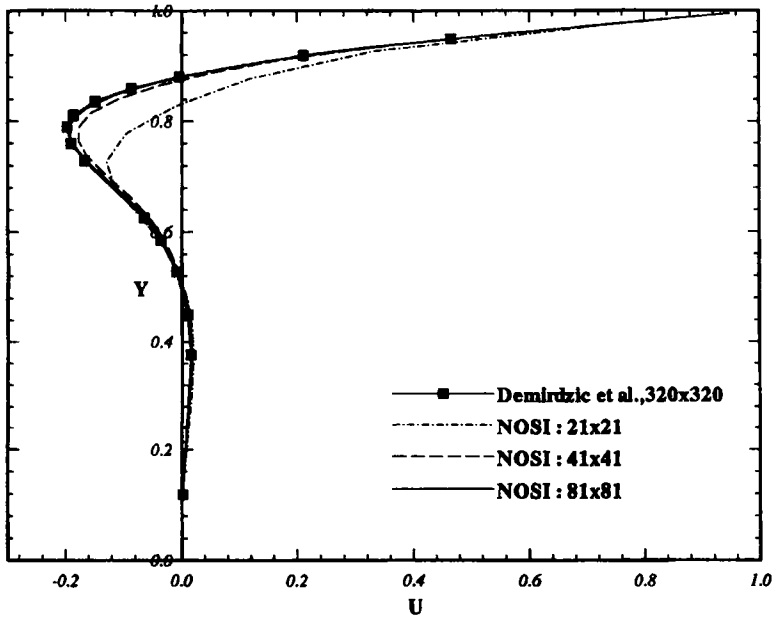

Figure 9(a). Velocity profiles of u along CL1 against grid density for $\theta = 30°$ and $Re = 1000$

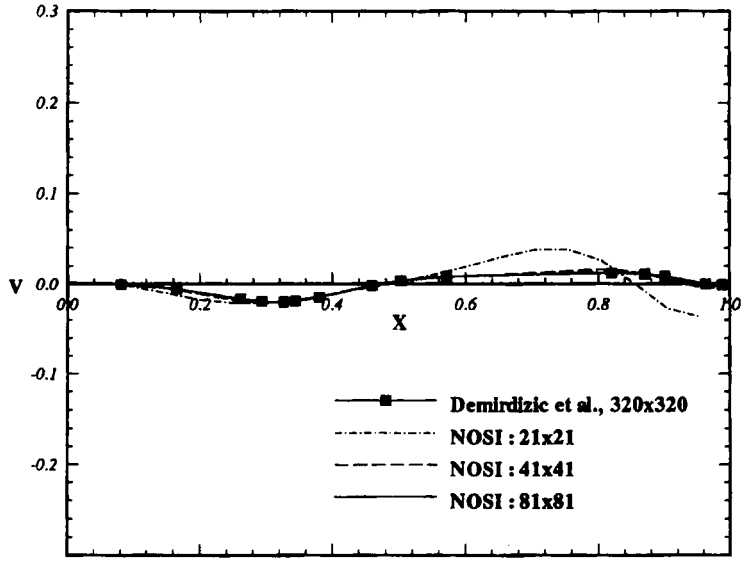

Figure 9(b). Velocity profiles of v along CL2 against grid density for $\theta = 30°$ and $Re = 1000$

As discussed earlier, difficulties do exist in utilizing the contravariant components, notably the sensitivity to grid curvature. The implications of the metric and indispensable source terms arising from the mapping between two co-ordinate systems must be considered. As a consequence, we estimated the computing cost associated with these aspects by considering the cavity flow problem with a tilt angle $\theta = \pi/2$. The computing costs on a grid system of 40 × 40 nodal points are plotted against the Reynolds number. Two grid systems have been investigated, namely the traditional uniform orthogonal grid and the curvilinear one which is shown in Figure 15. Based on calculations carried out

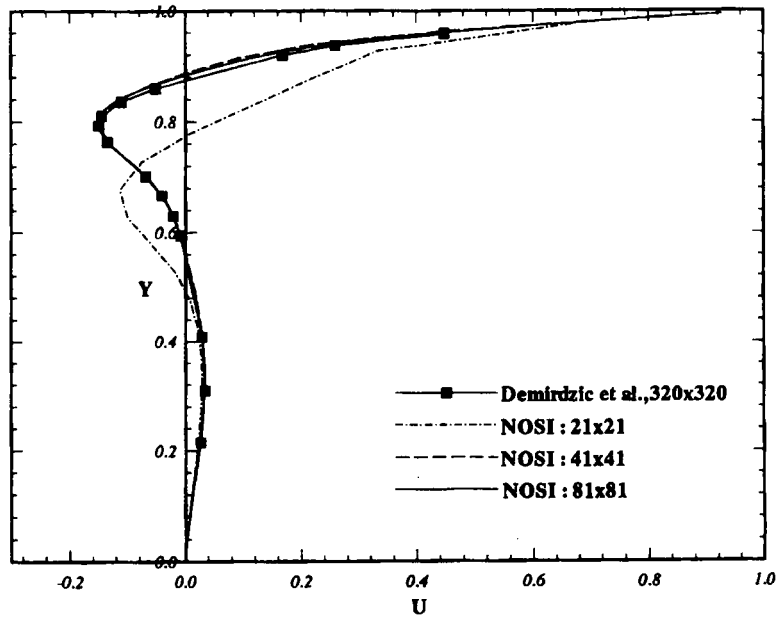

Figure 9(c). Velocity profiles of u along CL1 against grid density for $\theta = 45°$ and $Re = 1000$

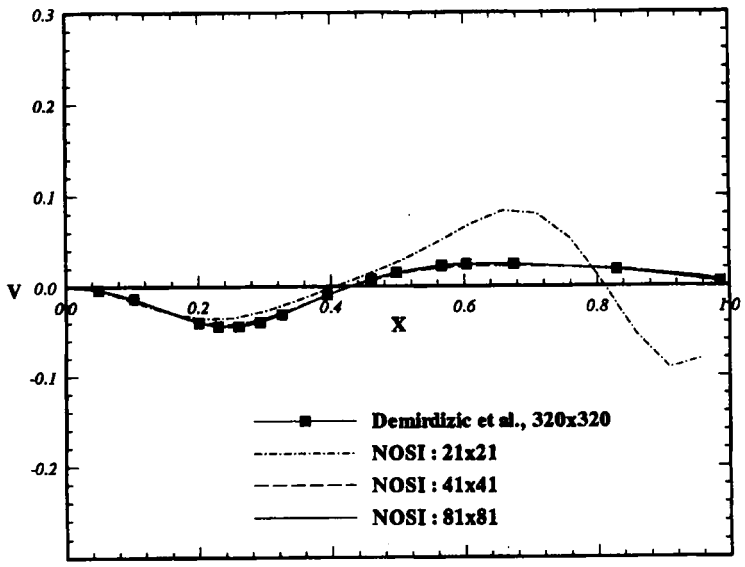

Figure 9(d). Velocity profiles of v along CL2 against grid density for $\theta = 45°$ and $Re = 1000$

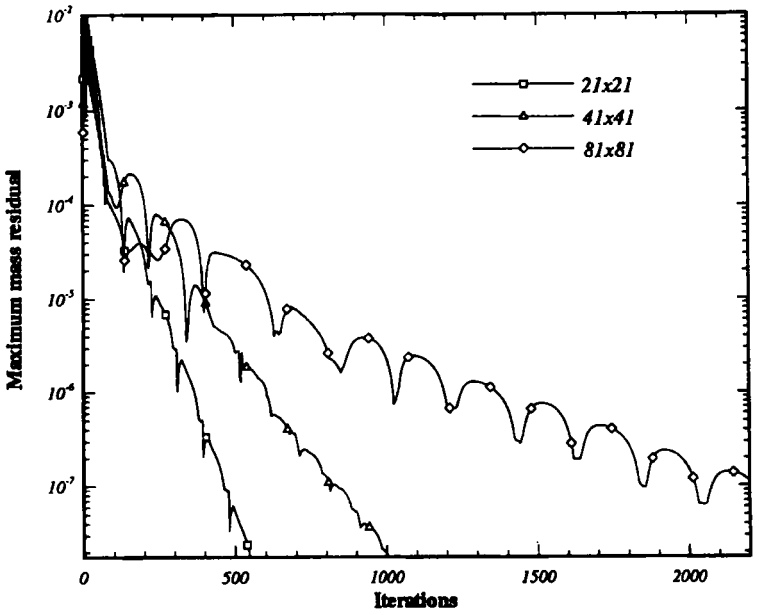

Figure 10(a). Comparison of convergence histories between three grid systems for $\theta = 30°$ and $Re = 100$ in terms of maximum mass residual

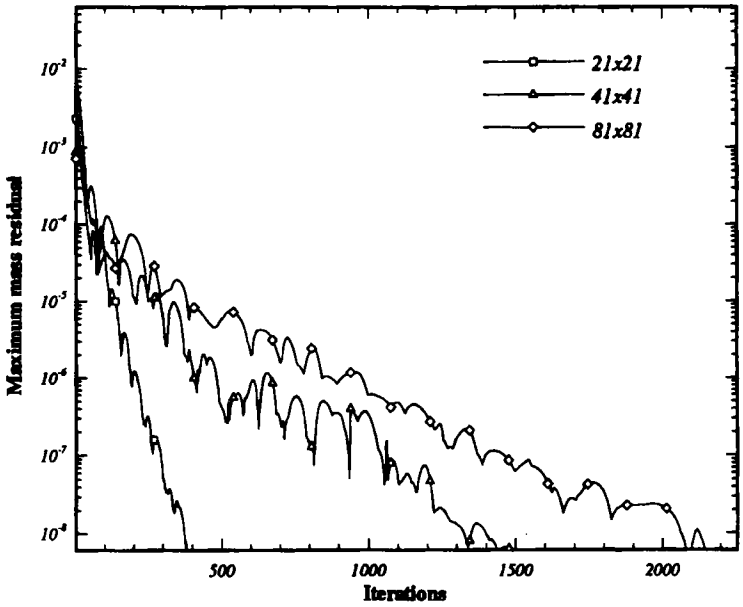

Figure 10(b). Comparison of convergence histories between three grid systems for $\theta = 45°$ and $Re = 100$ in terms of maximum mass residual

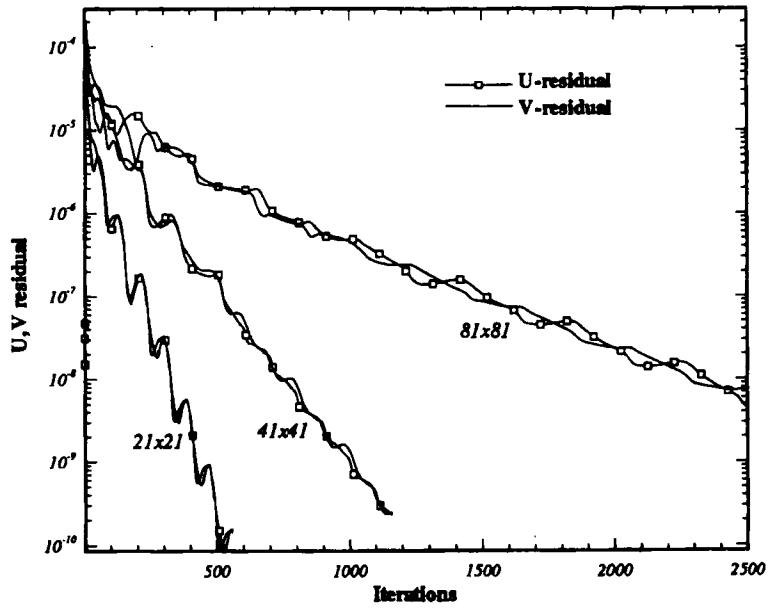

Figure 10(c). Comparison of convergence histories between three grid systems for $\theta = 30°$ and $Re = 100$ in terms of residuals of U and V

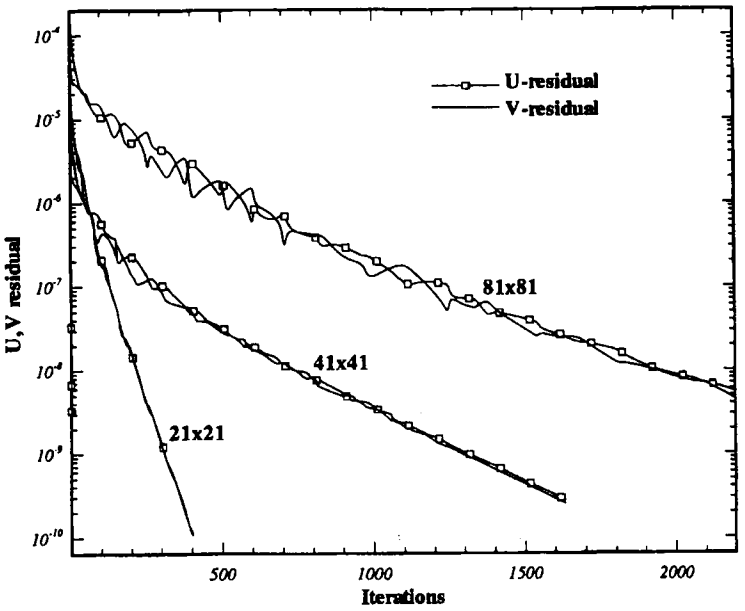

Figure 10(d). Comparison of convergence histories between three grid systems for $\theta = 45°$ and $Re = 100$ in terms of residuals of U and V

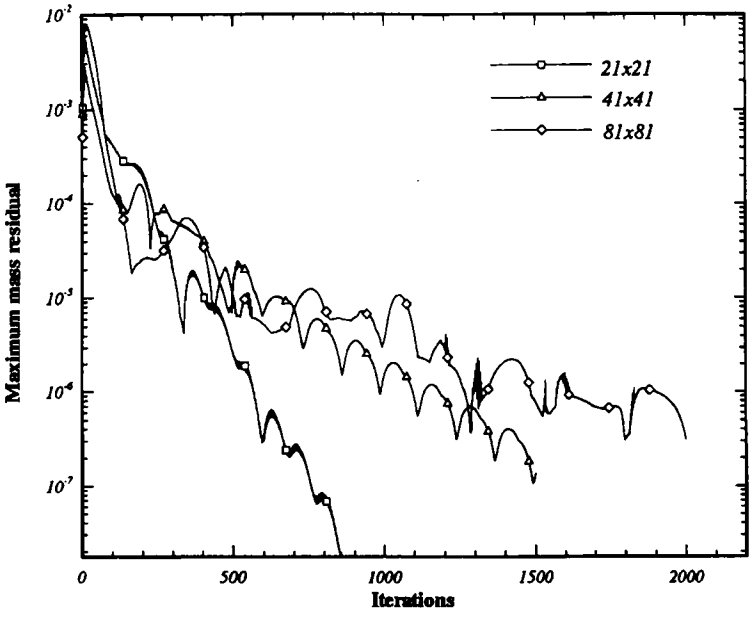

Figure 10(e). Comparison of convergence histories between three grid systems for $\theta = 30°$ and $Re = 1000$ in terms of maximum mass residual

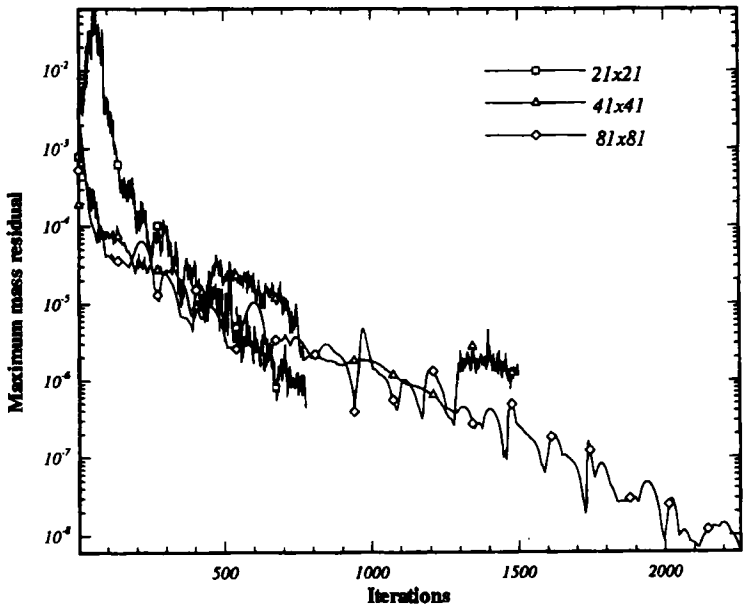

Figure 10(f). Comparison of convergence histories between three grid systems for $\theta = 45°$ and $Re = 1000$ in terms of maximum mass residual

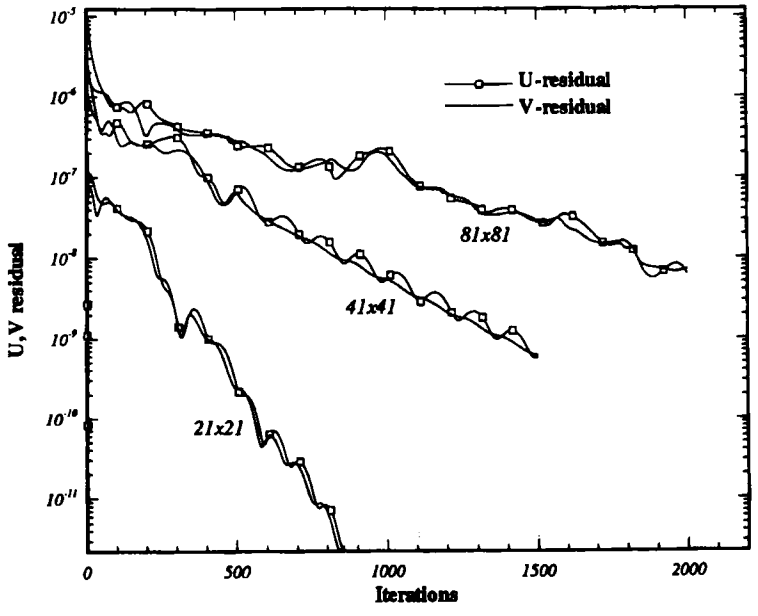

Figure 10(g). Comparison of convergence histories between three grid systems for $\theta = 30°$ and $Re = 1000$ in terms of residuals of U and V

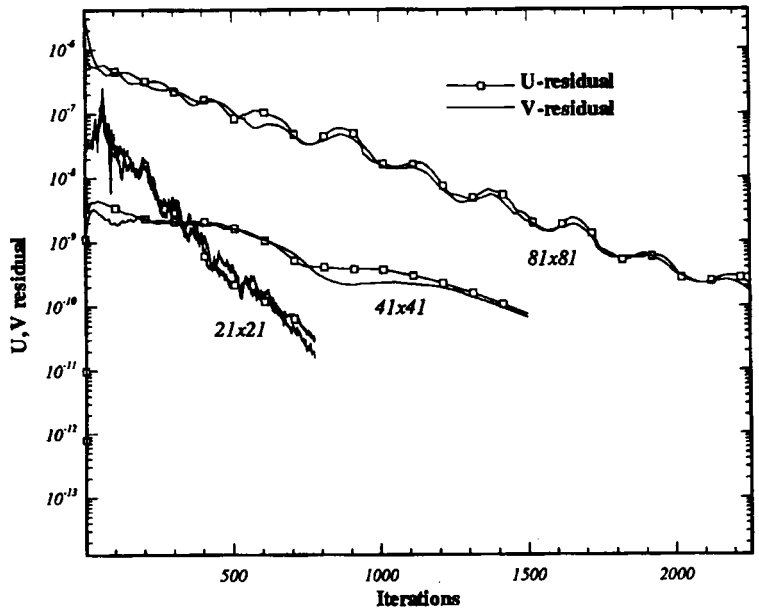

Figure 10(h). Comparison of convergence histories between three grid systems for $\theta = 45°$ and $Re = 1000$ in terms of residuals of U and V

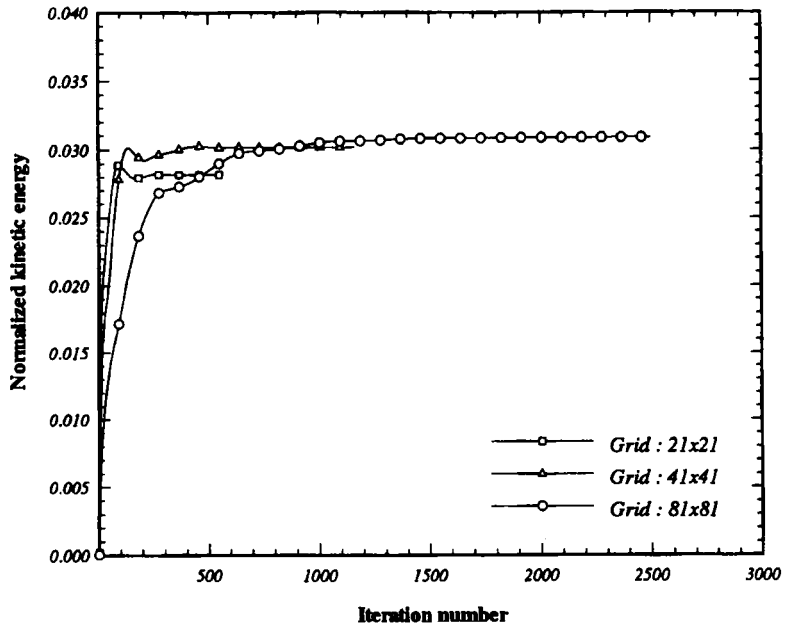

Figure 11(a). Comparison of convergence histories of kinetic energy between three grid systems for $\theta = 30°$ and $Re = 100$

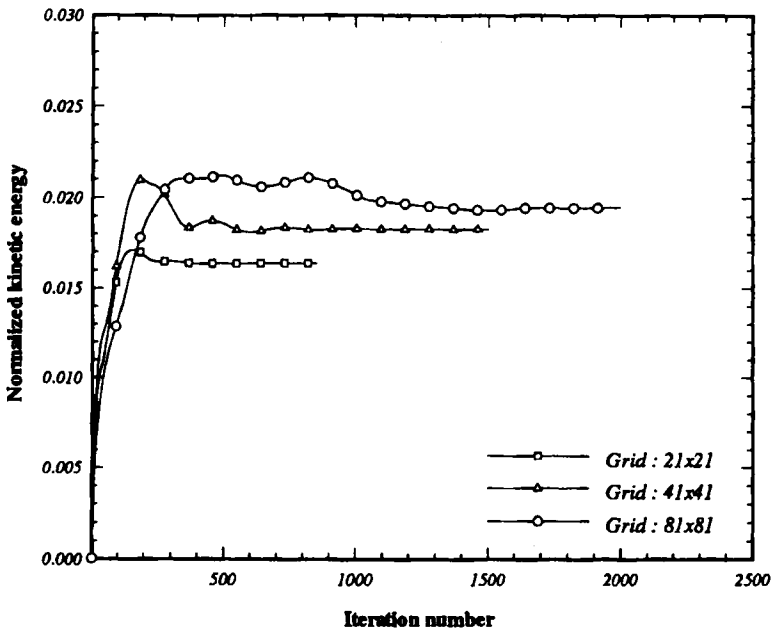

Figure 11(b). Comparison of convergence histories of kinetic energy between three grid systems for $\theta = 30°$ and $Re = 1000$

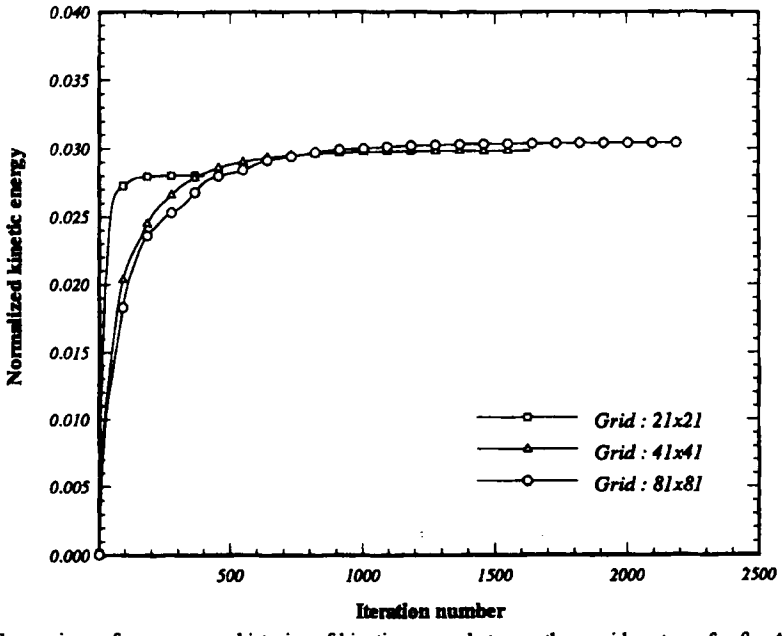

Figure 11(c). Comparison of convergence histories of kinetic energy between three grid systems for $\theta = 45°$ and $Re = 100$

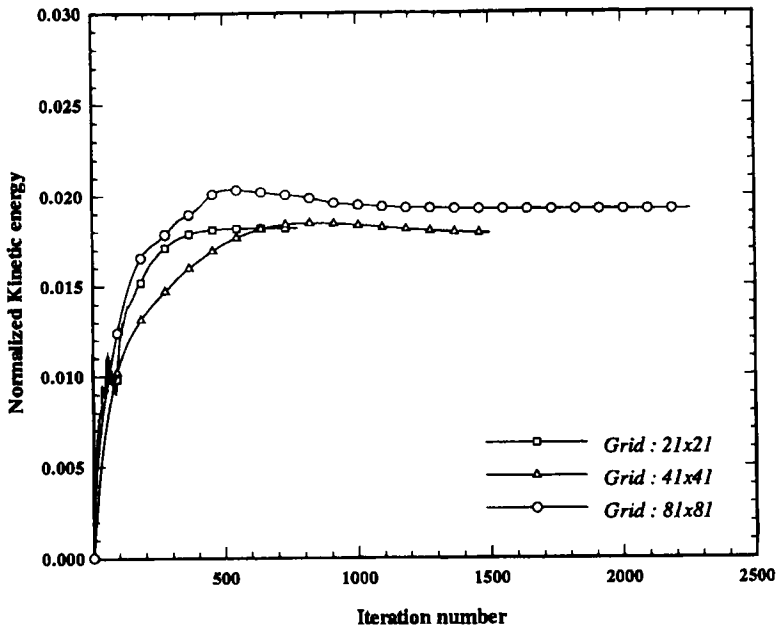

Figure 11(d). Comparison of convergence histories of kinetic energy between three grid systems for $\theta = 45°$ and $Re = 1000$

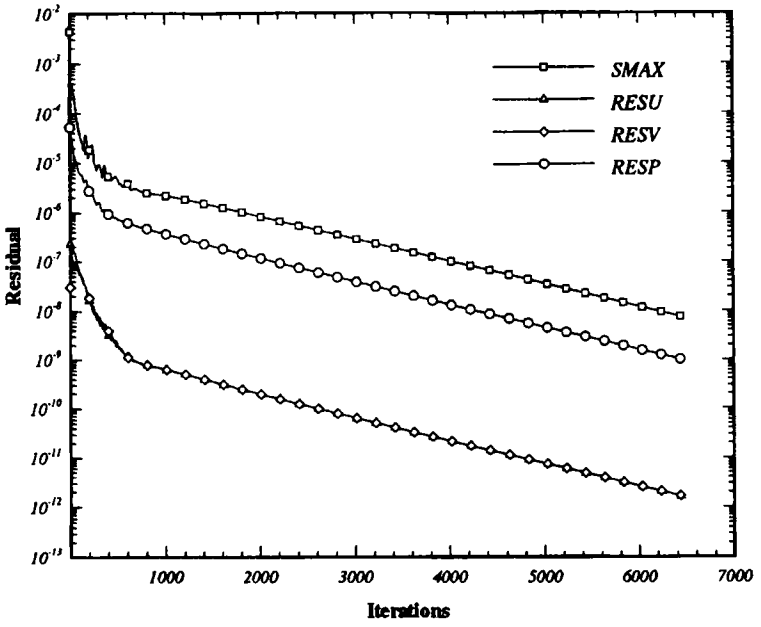

Figure 12. Convergence histories of U, V, P and maximum mass residuals of cavity flow at $Re = 3200$

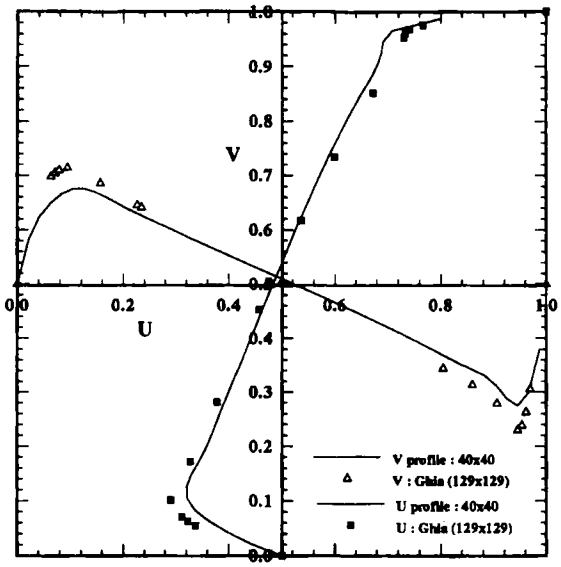

Figure 13. Comparison of U- and V-velocity profiles of cavity flow at $Re = 3200$

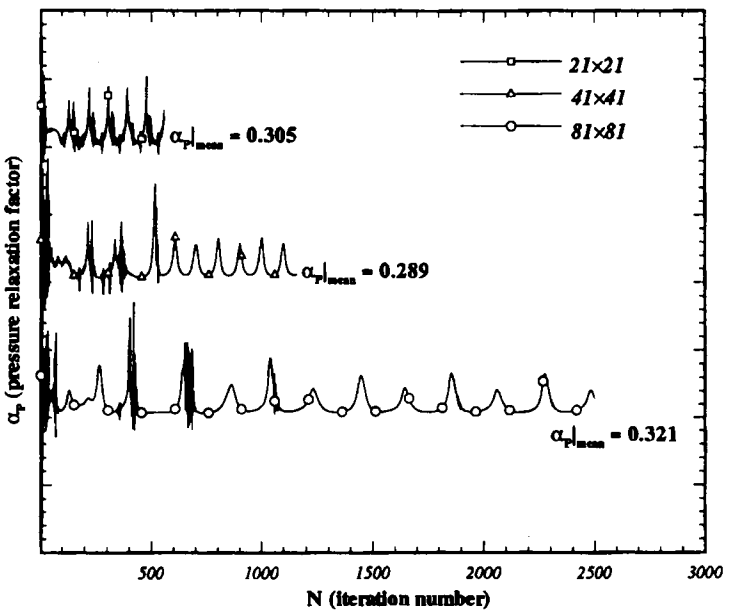

Figure 14(a). Comparison of pressure relaxation factors between three grid systems for $\theta = 30°$ and $Re = 100$

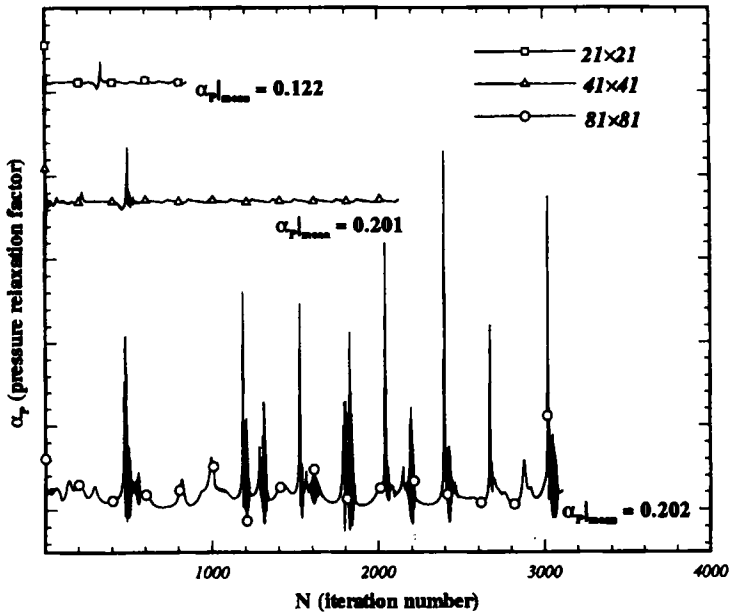

Figure 14(b). Comparison of pressure relaxation factors between three grid systems for $\theta = 30°$ and $Re = 1000$

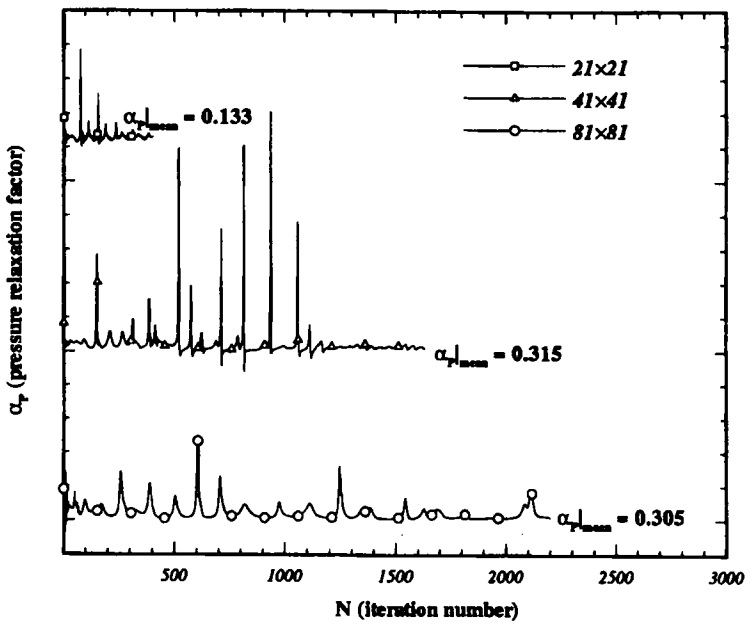

Figure 14(c). Comparison of pressure relaxation factors between three grid systems for $\theta = 45°$ and $Re = 100$

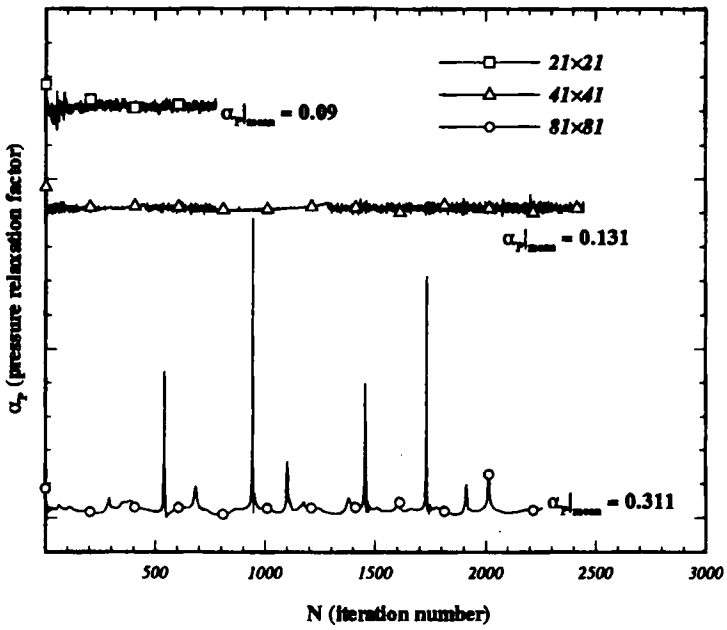

Figure 14(d). Comparison of pressure relaxation factors between three grid systems for $\theta = 45°$ and $Re = 1000$

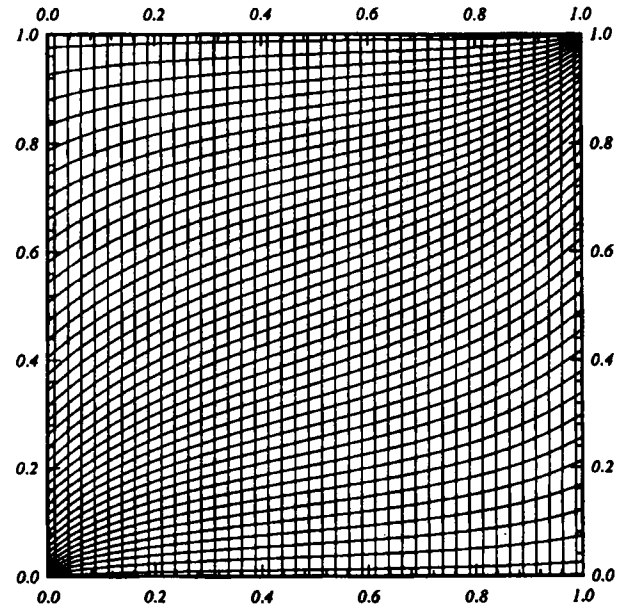

Figure 15. Grid system for driven cavity flow problem

on an Intel 486/DX33 personal computer with double precision, the difference in CPU time between curves 1 and 2 in Figure 16 corresponds to the extra cost needed for the evaluation of newly generated source terms, since the convergence histories are exactly the same. The deterioration of the convergence arising from the grid curvature is clearly seen from the difference in CPU time between curves 2 and 3 in Figure 16.

6.3. *Channel flow with a smooth expansion*

The problem depicted in Figure 17 was selected as the third test problem and also served as the target in the fifth workshop of the IAHR.[38] The problem is plausible in assessing the effectiveness of the proposed scheme both on Reynolds number and on mesh uniformity. The configuration of the investigated expansion channel is given by the expression

$$y_l = \left[\tanh\left(2 - \frac{30x}{Re}\right) - \tanh(2)\right]/2, \tag{32}$$

where $0 \leqslant x \leqslant x_{out} = Re/3$. At the bottom wall we specified the no-slip velocity condition. Owing to the flow symmetry, we only considered half of the domain, so that considerable computational time could be saved. At the centreline $\{(x, y) \mid 0 \leqslant x \leqslant x_{out}, y_u = 1\}$ we dictated that both the transverse gradient and the normal velocity component be zero in order to satisfy the condition of symmetry:

$$\frac{\partial u}{\partial n} = 0, \qquad v = 0. \tag{33}$$

At the inlet, $x = 0$ and $0 \leqslant y \leqslant 1$, we continuously supplied the liquid fluid with velocities given by

$$u = \tfrac{3}{2}(2y - y^2), \qquad v = 0. \tag{34}$$

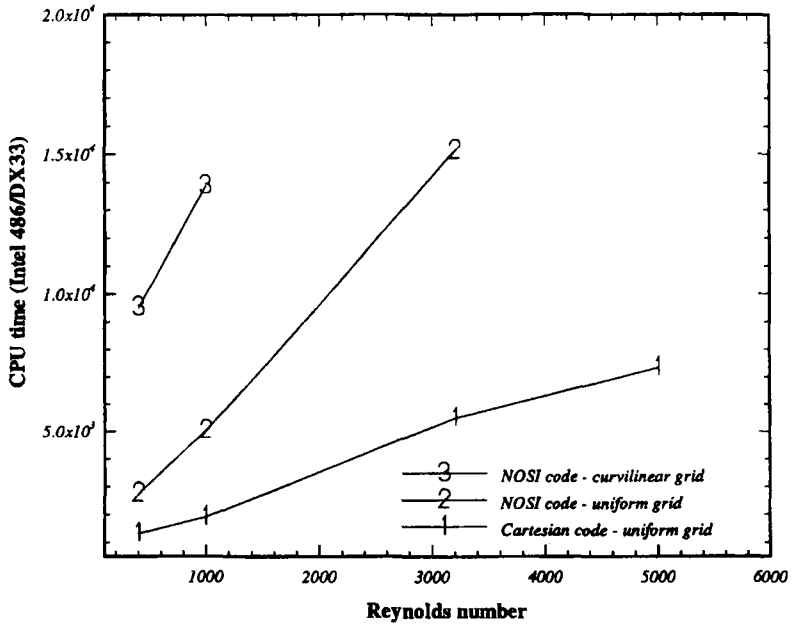

Figure 16. Comparison of CPU times for different analysis codes

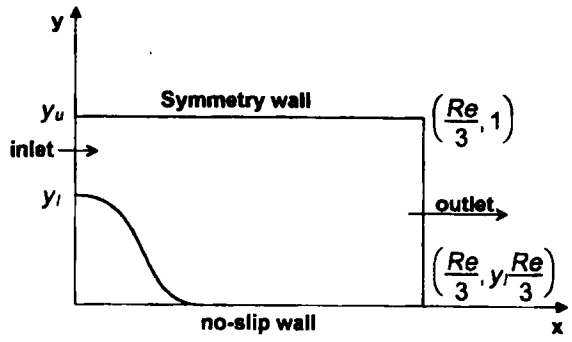

Figure 17. Schematic diagram of smooth expansion channel

For physical reasons we enforced the following boundary conditions at the exit in order to ensure mass conservation:

$$u_{i\max,j} = u_{im1,j}\left(\frac{\int_{j=1}^{j=j\max} u_{im1,j}\,dy}{\int_{j=1}^{j=j\max} u_{1,j}\,dy}\right), \qquad \left.\frac{\partial v}{\partial x}\right|_{i=i\max} = 0. \tag{35}$$

The working variables were solved for on mesh systems consisting of 21 × 21 and 41 × 41 grid nodes. Two Reynolds numbers, $Re = 10$ and 100 were studied. The former case was chosen to check the influence of the distorted geometry on the proposed method, the latter to assess the convergence rate concerning the value of Re. The computed pressures along the wall are illustrated in Figure 18, together with the results obtained by Cliffe *et al.*[38] The predicted values show good agreement with the benchmark solutions, except near the inlet. Also of note is that because the test Reynolds numbers are

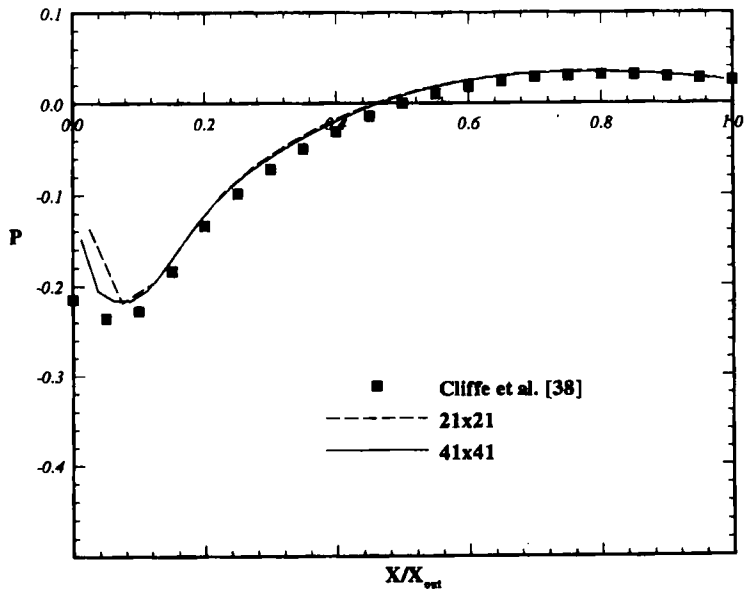

Figure 18(a). Pressure distributions along wall for $Re = 10$

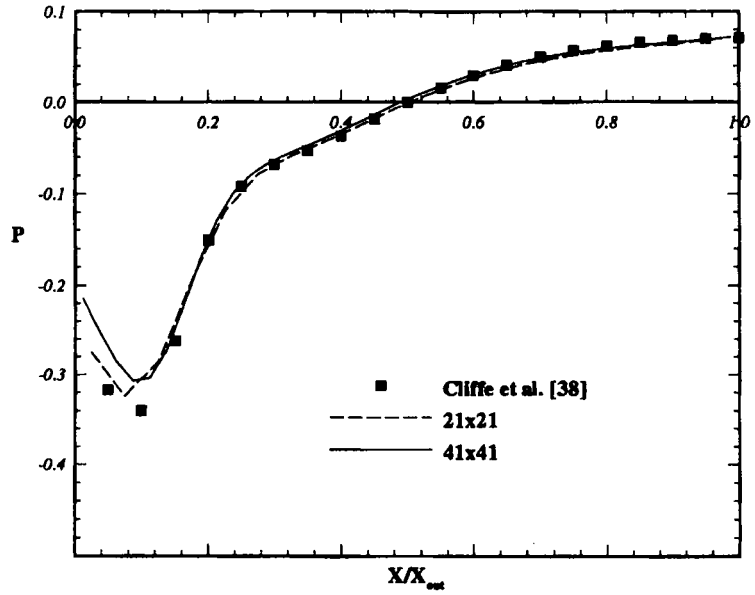

Figure 18(b). Pressure distributions along wall for $Re = 100$

small, the grid dependence does not necessarily show an appreciable variation between different Reynolds numbers.

The residuals in Figure 19 follow a reduction process similar to that discussed in the previous example. Also, we recorded the kinetic energy variations in Figure 20 to check whether flow steadiness can be reached. As shown in Figure 21, the computed relaxation factors change comparatively regularly at low Reynolds number if more grid nodes are engaged. The variations in these factors, on

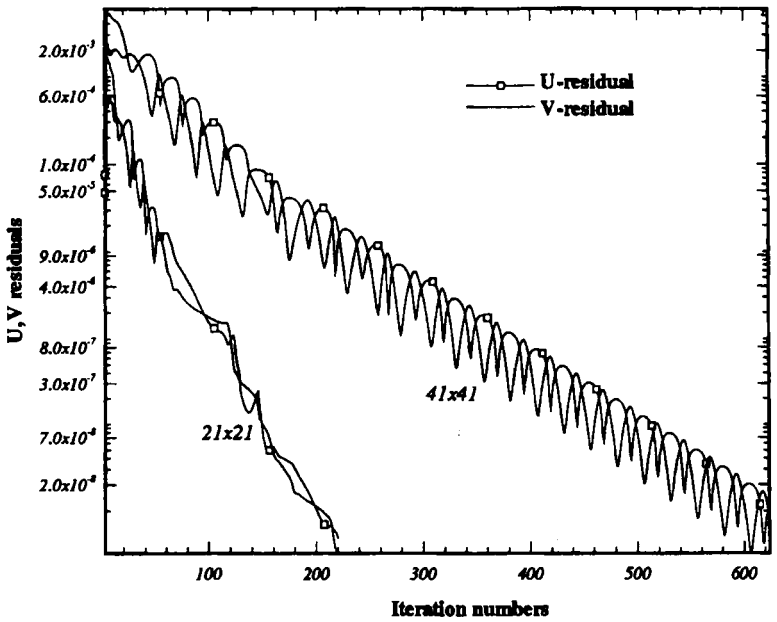

Figure 19(a). Comparison of convergence histories of U and V between two grid systems for $Re = 10$

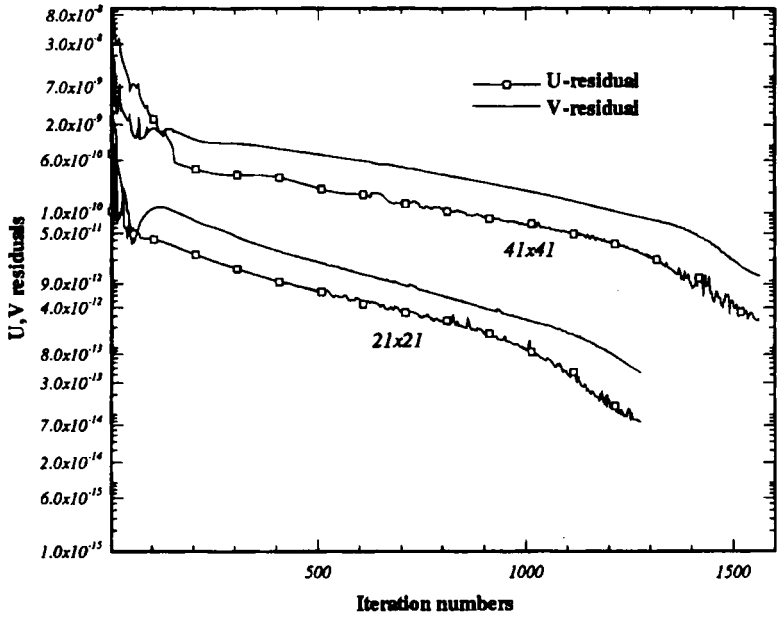

Figure 19(b). Comparison of convergence histories of U and V between two grid systems for $Re = 100$

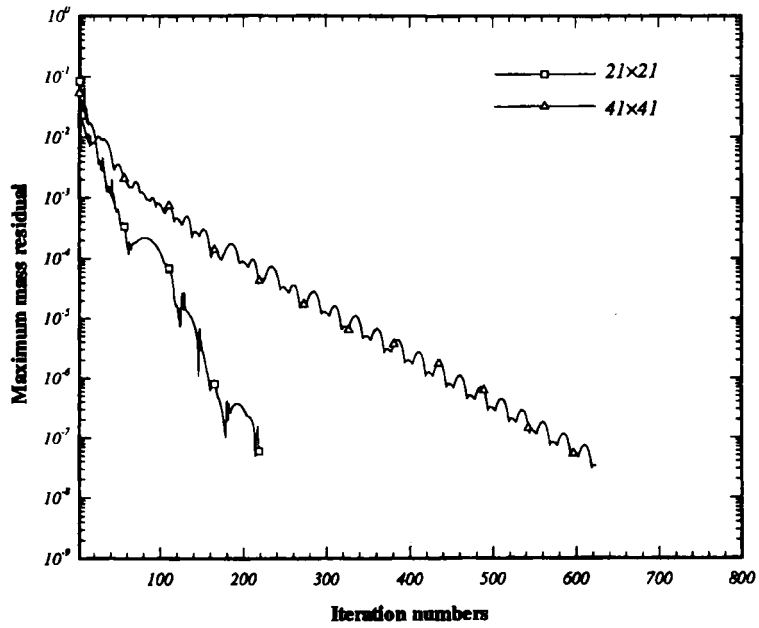

Figure 19(c). Comparison of convergence histories of maximum mass residual between two grid systems for $Re = 10$

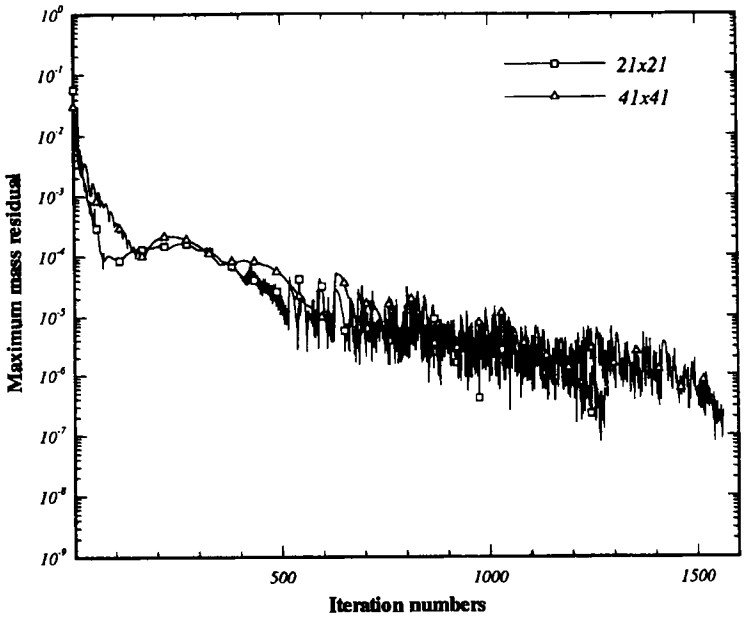

Figure 19(d). Comparison of convergence histories of maximum mass residual between two grid systems for $Re = 100$

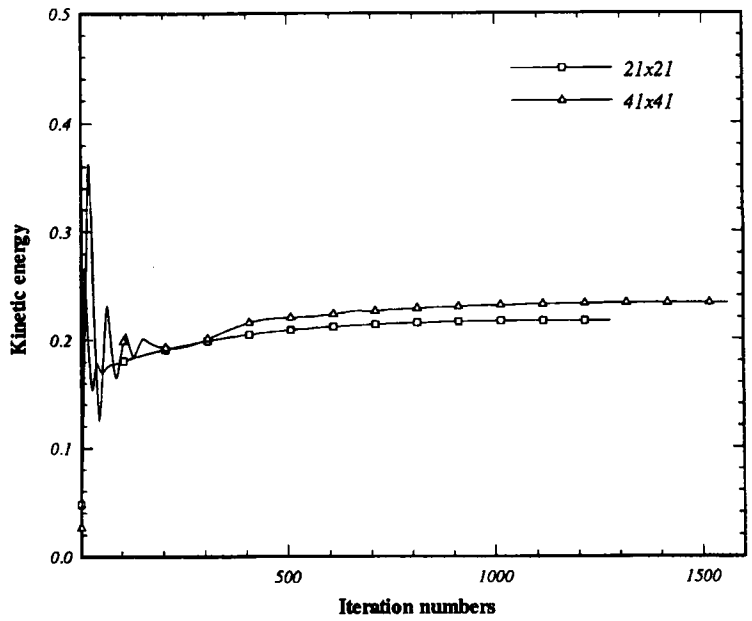

Figure 20(a). Convergence histories of kinetic energy for two grid systems for $Re = 10$

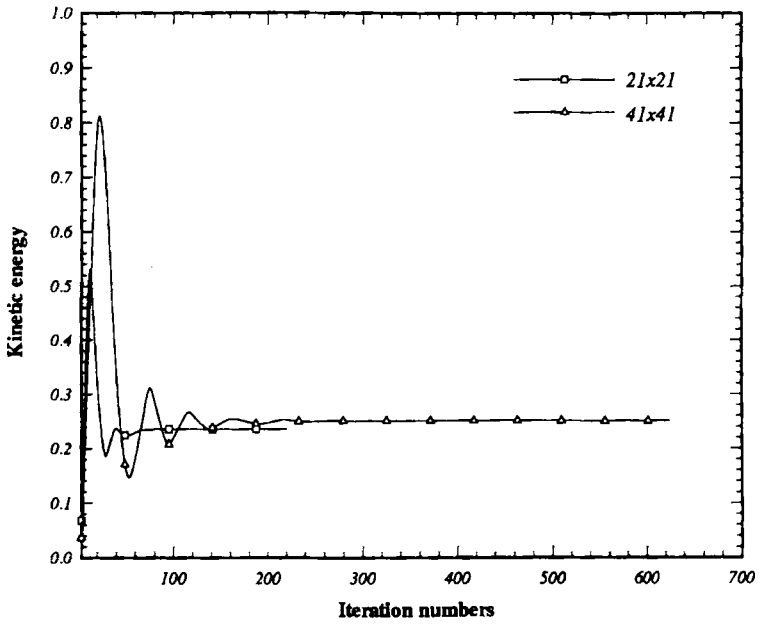

Figure 20(b). Convergence histories of kinetic energy for two grid systems for $Re = 100$

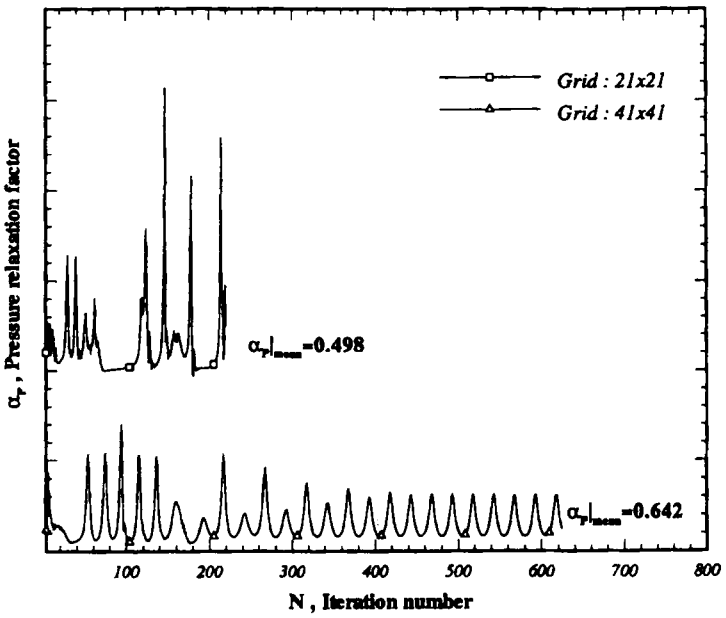

Figure 21(a). Relaxation factors of pressure for two grid systems for $Re = 10$

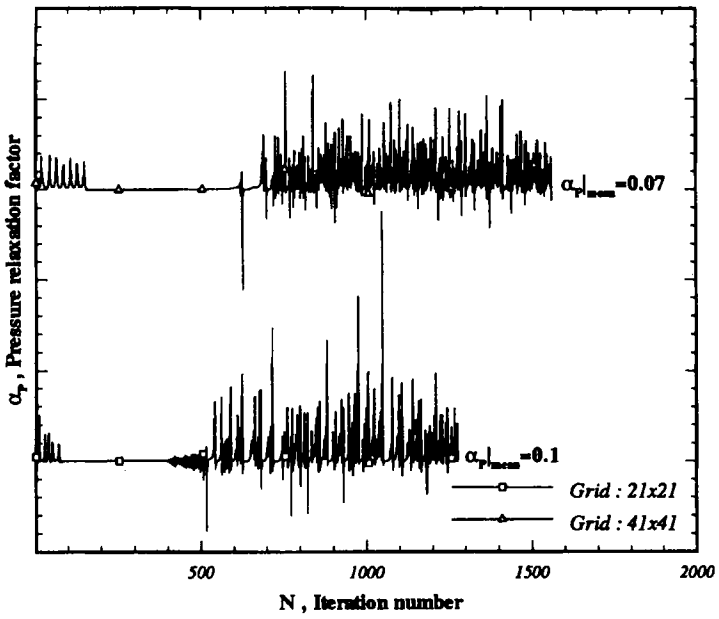

Figure 21(b). Relaxation factors of pressure for two grid systems for $Re = 100$

the other hand, become more severe as the Reynolds number increases, since the coefficient matrix becomes less diagonally dominant.

7. CONCLUSIONS

An extensive study on the present NO-SIMPLE-2D code has been conducted for an elliptic set of incompressible Navier–Stokes equations defined in a two-dimensional physical domain. The performances regarding solution accuracy as well as convergence rate have been the main concerns in this study. Major features and conclusions are as follows.

1. For geometrical reasons the contravariant components are retained in the equations as working variables. In the framework of body-fitted co-ordinate transformation, most analysts employ contravariant velocities only in the continuity equation for deriving the Poisson equation for the pressure or its correction. For the momentum equations we also choose contravariant velocity components as dependent variables. The solution quality computed on a mesh system of arbitrary shape will be the same as that yielded by Cartesian co-ordinates with a uniform mesh size if the metric data resulting from the co-ordinate transformation can be computed nearly analytically. As a consequence, methods capable of accurately computing these geometric quantities and maintaining the velocity transformations between the two grid systems as analytic as possible have been the theme of the present development. A major advantage in favour of using the contravariant velocity formulation is grounded in the fact that a simpler expression for the convective fluxes can be retained. This means that the non-linear flux terms that are responsible for the numerical instability can be more accurately discretized. In addition, it is advantageous to select a reliable discretization scheme, developed in the Cartesian co-ordinate system, and directly apply it to a computer programme formulated on the basis of contravariant velocities. For effectively reducing the false diffusion errors, a compact multidimensional 1/8 QUICK advection scheme involving a stencil of 13 points is utilized in this study.

2. For stability reasons the contravariant velocity components and pressure are stored in a staggered grid system to prevent even–odd pressure oscillations from occurring. The governing equations need discretizing at different cells in the present finite volume approach. The Cartesian velocity components, on the other hand, are collocated at the pressure node, so an interpolation procedure is indispensable.
3. The evaluation of curvature terms is indispensable provided that a body-fitted, non-orthogonal curvilinear co-ordinate transformation is implemented. The discretization accuracy therefore depends largely on how the contravariant/covariant base vectors, Christoffel symbols and Jacobian are approximated. In the present study the discretization accuracy has been demonstrated from the mathematical derivation as well as from the computed results.
4. Besides the analytic problem, both inflow–outflow and enclosure cavity flow problems have been investigated with success. As far as the grid sensitivity, measured in the skewness and resolution, and the Reynolds number of these problems are concerned, there exist different convergence routes to enlighten their importance. The effectiveness of employing the variable relaxation factor for the pressure equation was also demonstrated.

REFERENCES

1. A. Segal, P. Wesseling, J. Van Kan, C. W. Oosterlee and K. K. Kassels, 'Invariant discretization of the incompressible Navier–Stokes equations in boundary fitted coordinates' *Int. j. numer. methods fluids*, **15**, 411–426 (1992).
2. M. E. Braaten and W. Shyy, 'Comparison of iterative and direct solution methods for viscous flow calculation in body-fitted coordinates' *Int. j. numer. methods fluids*, **6**, 325–349 (1986).
3. S. V. Patankar, *Numerical Heat Transfer and Fluid Flow*, Hemisphere, Washington, DC, 1980.
4. F. H. Harlow and J. E. Welch, 'Numerical calculation of time-dependent viscous incompressible flow of fluid with free surface' *Phys. Fluids*, **8**, 2182–2189 (1965).
5. A. J. Chorin, 'A numerical method for solving incompressible viscous flow problems' *J. Comput. Phys.*, **2**, 12–26 (1967).
6. J. P. Van Doormaal and G. D. Raithby, 'Enhancements of the SIMPLE method for predicting incompressible fluid flows' *Numer. Heat Transfer*, **7**, 147–163 (1984).
7. S. V. Patankar, 'A calculation procedure for two-dimensional elliptic situations' *Numer. Heat Transfer*, **4**, 409–425 (1981).
8. R. Peyret and T. D. Taylor, *Computational Methods for Fluid Flow*, Springer, Berlin, 1983.
9. P. M. Gupta and R. P. Manohar, 'Boundary approximations and accuracy in viscous flow computations' *J. Comput. Phys.*, **31**, 265–288 (1979).
10. K. Azis and J. D. Hellums, 'Numerical solution of the three-dimensional equations of motion for laminar natural convection' *Phys. Fluids*, **10**, 314–324 (1967).
11. J. F. Thompson, Z. U. A. Warsi and C. W. Mastin, 'Boundary-fitted coordinate systems for numerical solution of partial differential equations — a review' *J. Comput. Phys.*, **47**, 1–108 (1982).
12. N. R. Patel and D. G. Briggs, 'A MAC scheme in boundary-fitted curvilinear coordinates' *Numer. Heat Transfer*, **6**, 383–394 (1983).
13. I. Demirdzic, A. D. Gosman, R. I. Issa and M. Peric, 'A calculation procedure for turbulent flow in complex geometries' *Comput. Fluids*, **15**, 251–273 (1987).
14. H. Q. Yang, K. T. Yang and J. R. Lloyd, 'Buoyant flow calculations with non-orthogonal curvilinear coordinates for vertical and horizontal parallelepiped enclosures' *Int. j. numer. methods eng.*, **25**, 331–345 (1988).
15. D. Lee and J. J. Chiu, 'Covariant velocity-based calculation procedure with nonstaggered grids for computation of pulsatile flows' *Numer. Heat Transfer B*, **21**, 269–286 (1992).
16. S. Koshizuka, Y. Oka and S. Kondo, 'A staggered differencing technique on boundary-fitted curvilinear grids for incompressible flows along curvilinear or slant walls' *Comput. Mech.*, **7**, 123–136 (1990).
17. T. Ikohagi, B. R. Shin and H. Daiguji, 'Application of an implicit time-marching scheme to a three-dimensional incompressible flow problem in curvilinear coordinate systems' *Comput. Fluids*, **21**, 163–175 (1992).
18. W. H. Sheu, Y. C. Liau, 'A space marching calculation method for three-dimensional flow problems' *Bull. College of Engineering, NTU, No. 49*, 1990, pp. 109–122.
19. W. H. Sheu and Y. C. Liau, 'Numerical prediction of free convection effects in an arbitrary cavity using SIMPLE family algorithms', in *Numerical Methods in Laminar and Turbulent Flow*, Vol. 6, Pt. 2, Pineridge, Swansea, 1989, pp. 1145–1155.
20. R. L. Meakin and R. L. Street, 'Simulation of environmental flow problems in geometrically complex domains. Part I: A general coordinate transformation' *Comput. Methods Appl. Mech. Eng.*, **68**, 151– 175 (1988).
21. G. de Vahl-Davis and G. D. Mallinson, 'An evaluation of upwind and central difference approximation by study of recirculating flows' *Comput. Fluids*, **4**, 24–42 (1976).
22. Y. Tamura and K. Fujii, 'A multi-dimensional upwind scheme for the Euler equations on structured grids' *Comput. Fluids*, **22**, 125–137 (1993).

23. W. H. Sheu, S. M. Lee and M. T. Wang, 'Multi-dimensional monotone flux discretization scheme for convection dominated flows', submitted to *Int. J. Heat Fluid Flow.*
24. C. W. Hirt, A. A. Amsden and J. C. Cook, 'An arbitrary Lagrangian–Eulerian computing method for all flow speed' *J. Comput. Phys.*, **2**, 12–26 (1967).
25. S. Abdallah, 'Numerical method for solving incompressible viscous flow problems' *J. Comput. Phys.*, **70**, 182–192 (1987).
26. S. Yoon and D. Kwak, 'Implicit Navier–Stokes solver for the three-dimensional compressible flows' *AIAA J.*, **30**, 2653–2659 (1992).
27. J. K. Dukowicz and A. S. Dvinsky, 'Approximate factorization as a high order splitting for the implicit incompressible flow equations' *J. Comput. Phys.*, **102**, 336–347 (1992).
28. A. A. Amsden and R. H. Harlow, 'The SMAC method: a numerical technique for calculating incompressible fluid flows' *Los Alamos Scientific Laboratory Rep. LA-4370*, 1970.
29. J. Van Kan, 'A second-order accurate pressure-correction scheme for viscous incompressible flow' *SIAM J. Sci. Stat. Comput.*, **7**, 870–891 (1986).
30. D. J. Jang, R. Jetli and S. Acharya, 'Comparison of the PISO, SIMPLER, and SIMPLEC algorithms for the treatment of the pressure–velocity coupling in steady flow problems' *Numer. Heat Transfer*, **10**, 209–228 (1986).
31. T. W. H. Sheu and S. M. Lee, 'A problem-independent segregates solution algorithm for incompressible flows in general coordinates' *Proc. 2nd Natl. Conf. on CFD*, 1993, pp. 445–450.
32. C. W. Oosterlee and P. Wesseling, 'A robust multigrid method for a discretization of the incompressible Navier–Stokes equations in general coordinates', in *Computational Fluid Dynamics '92*, Vol. 1, pp. 101–107, (1992).
33. G. Dhatt and G. Touzot, *The Finite Element Method Displayed*, Wiley, New York, 1984.
34. M. Braaten and W. Shyy, 'A study of recirculating flow computation using body-fitted coordinates: consistency aspects and mesh skewness' *Numer. Heat Transfer*, **9**, 559–574 (1986).
35. W. Shyy, S. S. Tong and S. M. Correa, 'Numerical recirculating flow calculation using a body-fitted coordinate system' *Numer. Heat Transfer*, **8**, 99–113 (1985).
36. I. Demirdzic, Z. Lilek and M. Peric, 'Fluid flow and heat transfer test problems for non-orthogonal grids: bench-mark solutions' *Int. j. numer. methods fluids*, **15**, 329–354 (1992).
37. U. Ghia, K. N. Ghia and C. T. Shin, 'High-Re solutions for incompressible flow using the Navier–Stokes equations and a multigrid method' *J. Comput. Phys.*, **48**, 387–411 (1982).
38. K. A. Cliffe, C. P. Jackson and A. C. Greenfield, 'Finite element solutions for flow in a symmetric channel with a smooth expansion', AERE-R. 10608.